NASA CONTRACTOR REPORT

NASA CR-1160

THE BUCKLING OF THIN-WALLED CIRCULAR CYLINDERS UNDER AXIAL COMPRESSION AND BENDING

by F. R. Stuart, J. T. Goto, and E. E. Sechler

Prepared by
CALIFORNIA INSTITUTE OF TECHNOLOGY
Pasadena, Calif.
for

NATIONAL AERONAUTICS AND SPACE ADMINISTRATION • WASHINGTON, D. C. • SEPTEMBER 1968

THE BUCKLING OF THIN-WALLED CIRCULAR CYLINDERS UNDER AXIAL COMPRESSION AND BENDING

By F. R. Stuart, J. T. Goto, and E. E. Sechler

Prepared under Grant No. NsG-18-59 by
CALIFORNIA INSTITUTE OF TECHNOLOGY
Pasadena, Calif.

for

NATIONAL AERONAUTICS AND SPACE ADMINISTRATION

For sale by the Clearinghouse for Federal Scientific and Technical Information
Springfield, Virginia 22151 – CFSTI price $3.00

THE BUCKLING OF THIN-WALLED CIRCULAR CYLINDERS UNDER AXIAL COMPRESSION AND BENDING

By F. R. Stuart, J. T. Goto, and E. E. Sechler

California Institute of Technology

SUMMARY

A series of tests was conducted on both electroplated copper and Mylar cylinders under combined axial compression and bending. Great care was taken to assure that the cylinders were as perfect as was possible and loading and boundary conditions were carefully controlled. For the Mylar cylinders, corrections were made for both area and stiffness of the lap joint. Under these conditions, much higher values of the buckling stress have been obtained than had been reported on by previous investigators.

INTRODUCTION

As an extension of the work on the buckling stress of thin-walled circular cylinders, it was desirable to determine the effects of combined loading conditions. One of the most important of these from a structural design standpoint is the combination of axial load and bending. By using an electroplating technique discussed in References 1, 2, and 3, thin-walled cylinders could be made without seams, with a high degree of dimensional accuracy, and which had a minimum of initial deformations. In addition to the tests on these "perfect" metal cylinders, a number of tests were run on cylinders made from Mylar. These cylinders had a lap seam whose dimensions were varied. The main difference between these tests on Mylar specimens and those carried out by other experimenters lay in the fact that the effect of both the area and the stiffness of the seam were taken into account in reducing the experimental data. Loading and boundary conditions were carefully controlled and any anomalies in the data were systematically investigated.

The combination of axial compression and bending, even though it is a common loading for both aircraft and missiles, has not been extensively investigated. References 4 and 5 give interaction data for this loading condition for celluloid and Mylar cylinders with a few check points in reference 4 for metal specimens. Even the case for pure bending has been in doubt since, until recently, the theoretical value of critical bending stress was accepted as that presented by Flügge, namely $1.3\,\sigma_c$ (Ref. 6). It has been shown (Ref. 7) that Flügge's calculation was quite restricted and a more general investigation has led to the conclusion that the maximum stress to cause bending failure is the same as that necessary to cause failure under uniform axial compression.

In the past, experimental investigations have been discouraging. The correspondence with theory was poor (Ref. 8) and the scatter has been great. However, it has been shown by Babcock that careful fabrication of the test specimens and good control of the experimentation will lead to more satisfactory results. These controls have been practiced in the current set of tests.

The Metal Specimens

The electroforming process discussed in Reference 1 was used. Briefly, the method consists of plating a copper shell on an accurately machined 8.0 inch (20.3 cm) diameter form which has been coated with silver paint. After plating, the shell is cut to a length of 10 inches (25.4 cm) and is removed by melting the wax. Specimen dimensions are shown in Table I.

The average thickness of the shell was found by accurately weighing the shell and dividing this weight by the surface area and density. A density of 8.9 grams/cc (8900 kg/m^3) was used for this purpose and checks of the actual thickness using a comparator on samples confirmed the method. Spot checks on typical cylinders indicated that the variation in thickness over the shell area was not greater than $\pm$ 3 o/o. See Table II for typical results.

Poisson's Ratio was taken as 0.30 and the modulus of elasticity was measured by specimens from each shell which were tested in

uniaxial tension on an Instron testing machine. A typical stress-strain curve is shown in Fig. 1 which indicates good linearity up to a stress value of about 13,000 psi (89.6 MN/m^2). The value of Young's modulus used to reduce the data is an average of several tests conducted on specimens from each shell. These values are shown in Table III. Table III also indicates the scatter obtained during these tests. Similar values for electroplated copper were obtained by Read and Graham (Ref. 9) and they explained the scatter by the grain size of different specimens.

After mounting the base of the specimen in the testing machine, measurements were taken to determine the deviation of the cylinder generators from a straight line. The pick-up was an iron-core reluctance unit with an output of approximately 25 volts/inch (10 volts/cm) and had a working range of 0.200 inches (7.87 mm). It was mounted on a vertical slide that could be placed at any place desired around the circumference, Fig. 2. Figs. 3, 4, and 5 show typical data.

Test Procedure for Metal Cylinders

The cylindrical shell was first mounted in a brass end ring with a low temperature melting point alloy, Cerrobend. After the Cerrobend hardened, the other end of the shell was mounted in the load ring of the testing machine with the same material. The testing machine was then rotated to the testing position (horizontal) and the free end of the shell (that opposite to the load ring) was rigidly attached to the machine end plate with Devcon Plastic Steel. Figure 6 shows the testing machine and shell in the testing position.

Although the testing machine was originally designed for axial loading it was possible to apply a bending moment by varying the end plate displacement through non-uniform adjustment of the three loading screws. Close control of the end plate movement was possible since a single revolution of the loading screws corresponded to 0.025 inch (0.635 mm) and the screw could be adjusted to one tooth of the 180 tooth loading gear.

The total applied load and the load distribution was obtained from the loading ring, Fig. 7. This was a brass cylinder 8.00 inches

(20.32 cm) in diameter, 2.50 inches (6.35 cm) long and 0.0107 inches (0.271 mm) thick. Twenty-four strain gages were mounted around the inside and outside circumference at equally spaced stations – inside and outside gages being directly opposite each other. The load ring gages were connected into a bridge circuit with dummy gages on a brass plate to give temperature compensation. The output was connected to an amplifier and read out on a Leeds and Northrop voltmeter. The load ring was calibrated to determine the load and moment as a function of gage output. Typical calibration curves are shown in Fig. 8.

The actual testing was carried out in the following manner: After the shell was mounted, the desired difference in strain gage readings was adjusted at diametrically opposite points in the shell. Once the desired moment was applied, all three loading screws were operated simultaneously to apply uniform axial compression. Data were taken at approximately 50 $^{o}/o$ of the anticipated buckling load and at small increments thereafter. If necessary, individual screw adjustments were made to maintain the desired bending moment. The axial compression load was increased until buckling occurred and the highest strain gage readings were recorded.

Test Results on Metal Cylinders

A total of 16 shells were tested. Table I gives the description of the specimens and Table V a summary of the results. The data are shown plotted in Fig. 9 in which

$$C_b = \sigma_b R/Et \qquad C_c = \sigma_c R/Et \qquad C_\sigma = 0.6 = \sigma_{c\ell} R/Et \tag{1}$$

where

σ_b = maximum bending stress

σ_c = uniform compressive stress

$\sigma_{c\ell}$ = classical buckling stress

Buckling occurred in all tests with complete failure and subsequent large load reduction. There were no visual indications of local buckling before failure. The postbuckling state was the familiar diamond shaped pattern occurring in several rows around the circumference in most cases. When high moments were present, buckling was restricted to the high stress side of the shell.

Strain gage data was reduced by a Fourier analysis carried out on an IBM 7094 computer. The method employed was that of Reference 10. The data were presented in the form

$$\text{strain gage reading} = A_o + \sum_{M=1}^{6} B_n \cos(\theta - \phi_n) \qquad (2)$$

and the constant and the first harmonic coefficients were used to calculate the applied loads and stresses. Table IV gives the results of this analysis and Figs. 10 and 11 show typical correspondence between the actual strain gage readings and the Fourier representation used to calculate the buckling stresses.

A few metal cylinders were tested under dead-weight loading, in contrast to a fixed displacement loading. These are also shown in Fig. 9 and the data show the same trend as those obtained earlier.

Another method of presenting the data is shown in Fig. 12 where $\sigma_{TOT}/\sigma_{c\ell}$ is plotted against $\sigma_b/\sigma_{c\ell}$ where

$$\sigma_{TOT} = \sigma_c + \sigma_b$$

Conclusions Concerning Metal Cylinders

Figures 9 and 10 indicate that careful testing of carefully made metal cylinders will give much higher values for the buckling stresses than have been reported on previously. In general, the total stress that can be developed lies between 0.65 and 0.95 times the classical buckling stress, the higher values being obtained for loads approaching pure bending. There may be two reasons for this trend namely:

a) The high stresses for pure bending are acting over a smaller percentage of the total shell and,

b) The effect of the fixed boundary as discussed in Reference 3 may be different for bending than it is in uniform axial compression and may not be as effective in lowering the buckling stress.

The Mylar Specimens

A second program on the same problem was set up using cylinders made of Mylar. The advantage in using this material is that, if postbuckling is not carried too far, the specimen does not suffer permanent damage upon buckling and can, therefore, be used to obtain many data points.

The specimens were 8 inches (20.32 cm) in diameter and 10 inches (25.40 cm) long and had thicknesses ranging from 0.00475 to 0.0103 inches (0.1206 to 0.2616 mm). The ends were cast in a circular slot in an aluminum end plate using Cerrolow, a low melting point alloy. In order to assure that the Mylar did not slip in the alloy (particularly when the sheet was in tension) it was found necessary to add a locking device to the edge. This was easily accomplished by putting a row of paper staples around the edge so that they would be buried in the Cerrolow.

Loading was through a ring dynamometer and was accomplished by a hand-turned, fine thread screw attached to the frame of the testing machine. The ring dynamometer was calibrated with dead weights. Load points all lay along a diameter containing the seam and the combined loading consisted of an axial compressive load equal to (See Fig. 13)

$$P_A = P_L + P_H$$

where P_L = the load read by the dynamometer plus the dynamometer dead weight and

P_H = the dead weight of the loading head.

To this is added a bending moment given by

$$M = P_L \times e \pm P_H \times \delta e$$

where

e = the distance of the loading point from the experimentally determined neutral axis and

δe = the distance from the center line of the specimen to the neutral axis.

The seams were made as an overlap cemented with an Epoxy cement. Since the combination of Epoxy and Mylar did not have the same Young's modulus as the Mylar alone, typical seams were cut from specimens and tested in uniaxial tension to determine the seam modulus, E_s. From this value and the seam dimensions a theoretical neutral axis and an effective area could be calculated as indicated in the Appendix. In addition to the theoretical neutral axis, an experimental one was determined by finding that loading point which gave the maximum axial load carrying ability of the specimen. Curves for the 7 specimens tested are shown in Fig. 14. Since the experimental determination of the neutral axis also took into account any effect of seam initial waviness, the experimental value was used to calculate the bending moments and the bending stresses.

Test Results on Mylar Cylinders

Table VII gives the stress ratios for the seven Mylar cylinders tested and the results are plotted in Figs. 19 to 21 inclusive. In general, there is a linear relationship between $\sigma_c/\sigma_{c\ell}$ and $\sigma_b/\sigma_{c\ell}$ and the maximum allowable total stress remains nearly constant. As in the metal cylinders, when the stress is primarily due to bending, the buckling stress is somewhat higher than it is when a uniform axial compressive stress is acting. Even so, the increase is not great and it would be conservative, but not excessively so, to use the same value for the allowable maximum bending stress as is found for uniform axial compression.

Collected summary data for the two smallest R/t ratios are shown in Figs. 22 and 23 and the summary for the total stress ratios are shown in Fig. 24. Finally, the collection of all data collected in this study both on Mylar and metal cylinders is shown in Fig. 25 in comparison with previously existing data.

CONCLUSIONS

The following conclusions appear valid as a result of this study on combined axial and bending loads on circular cylinders:

1) By using careful control over specimen and testing technique variables, much higher values of cylinder buckling stresses can be obtained than have been previously reported. This is true, not only for seamless metal cylinders made by a plating process, but also for Mylar cylinders having a lap seam.

2) The buckling stress for bending can conservatively be assumed to be the same as that found by tests on cylinders loaded with uniform axial compression.

3) When the maximum total stress is on the seam side of such cylinders the buckling stress may be lower than when the maximum stress is opposite to the seam, but it still has a value equal to that found in pure compression.

4) Detailed study of the effect of the boundary conditions on cylinders under bending appears to be called for.

APPENDIX

Correction equations for the effect of the seam on the moment and stress analysis.

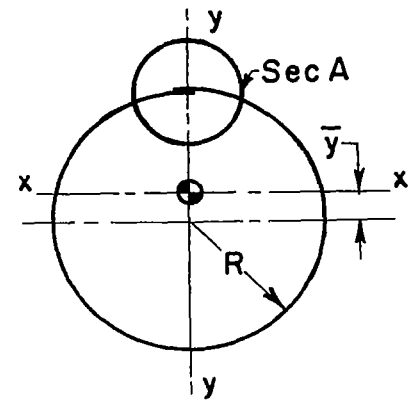

Letting

t = thickness of cylinder wall

w_s = width of seam

t_s = thickness of seam

R = cylinder radius

E = Young's modulus of cylinder material

E_s = Young's modulus of seam

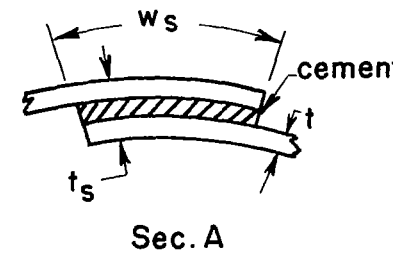

Then the effective area is

$$A_e = 2\pi Rt - w_s t + w_s(t_s \frac{E_s}{E})$$

$$= 2\pi Rt + w_s t_s (\frac{E_s}{E} - \frac{t}{t_s}) \qquad (A\text{-}1)$$

The distance to the neutral axis is

$$y = w_s t_s(\frac{E_s}{E} - \frac{t}{t_s})(R + \frac{t_s}{2}) / A_e \approx w_s t_s(\frac{E_s}{E} - \frac{t}{t_s})R/A_e \qquad (A\text{-}2)$$

since $\frac{t_s}{2} << R$.

The moment of inertia about x-x axis is given by

$$I_{xx} = \pi R^3 t + 2\pi Rt\bar{y}^2 + w_s t_s(\frac{E_s}{E} - \frac{t}{t_s})(R - \bar{y})^2 \qquad (A\text{-}3)$$

and, about the y-y axis is

$$I_{yy} = \pi R^3 t + \frac{w_s^3 t_s}{12}\left[\frac{E_s}{E} - \frac{t}{t_s}\right] \qquad (A\text{-}4)$$

Conversion of U. S. Customary Units to SI Units

The International System of Units (SI) was adopted by the Eleventh General Conference on Weights and Measures, Paris, October 1960, in Resolution No. 12, Ref. 11. Conversion factors for the units used herein are given in the following table:

Physical Quantity	U.S. Customary Unit	Factor (*)	SI Unit
Density	lbm/ft^3	16.02	$kilograms/meter^3 (kg/m^3)$
Force	lbf	4.448	newtons (N)
Length	in.	0.0254	meters (m)
	in.	2.54	centimeters (cm)
	in.	25.4	millimeters (mm)
Stress	$psi=lbf/m^3$	6.895×10^3	$newtons/meter^2 (N/m^2)$
Area	$in.^2$	645.2	$millimeters^2 (mm^2)$
Moment of Inertia	in^4	4.163×10^4	$millimeters^4 (mm^4)$
Bending moment	in-lbf	0.1130	meter-newtons (m-N)

* Multiply value given in U.S. Customary Unit by conversion factor to obtain equivalent value in SI Unit.

Prefixes used

giga (G) = 10^9

mega (M) = 10^6

centi (c) = 10^{-2}

milli (m) = 10^{-3}

REFERENCES

1. Babcock, C. D.: The Buckling of Cylindrical Shells with an Initial Imperfection under Axial Compression Loading. Ph. D. Thesis, California Institute of Technology, 1962.
2. Babcock, C. D. and Sechler, E. E.: The Effect of Initial Imperfections on the Buckling Stress of Cylindrical Shells. NASA TN 2005, July 1963.
3. Babcock, C. D. and Sechler, E. E.: The Effect of End Slope on the Buckling Stress of Cylindrical Shells. NASA TN D-2537, December 1964.
4. Bruhn, E. F.: Tests on Thin-Walled Celluloid Cylinders to Determine the Interaction Curves under Combined Bending, Torsion, and Compression or Tension Loads. NACA TN 951, January 1945.
5. Weingarten, V. I., Morgan, E. J., and Seide, P.: Final Report on Development of Design Criteria for Elastic Stability of Thin Shell Structures. Space Technology Laboratories, Report No. STL/TR-60-0000-19425 (EM 10-26), December 1960, pp. 127-132.
6. Flügge, W.: Die Stabilitaet der Kreiszylinderschale. Ingen. Archiv., Vol. 3, 1932, pp. 463-506.
7. Seide, P., and Weingarten, V. I.: On the Buckling of Circular Cylindrical Shells under Pure Bending. Space Technology Laboratories, Report No. TR-59-0000-00688 (EM 4-11), June 1959.
8. Fung, Y. C., and Sechler, E. E.: Instability of Thin Elastic Shells. Structural Mechanics, Pergamon Press, Oxford, London, 1960, pp. 115-116.
9. Read, H. J., and Graham, A. H.: The Elastic Modulus and Internal Friction of Electrodeposited Copper. Journ. of Electro-Chemical Society, Vol. 108, No. 2, 1961.
10. von Kármán, T.: and Biot, M.: Mathematical Methods in Engineering, McGraw-Hill Book Co., Inc., New York, 1940, pp. 336-338.
11. Mechtly, E. A.: The International System of Units – Physical Constants and Conversion Factors. NASA SP-7012, 1964.

TABLE I

DESCRIPTION OF TEST SPECIMENS

Shell	Length		Thickness		R/t
	inches	(cm)	inches x 10^3	(mm)	
S-1	9.97	(25.32)	4.78	(0.121)	838
S-2	9.98	(25.34)	4.69	(0.119)	855
S-3	10.03	(25.48)	4.97	(0.126)	805
S-4	9.97	(25.32)	4.78	(0.121)	838
S-5	9.98	(25.34)	4.68	(0.119)	855
S-6	10.00	(25.40)	4.91	(0.125)	815
S-7	10.00	(25.40)	4.60	(0.117)	870
S-8	9.97	(25.32)	4.78	(0.121)	836
S-9	9.97	(25.32)	4.85	(0.123)	825
S-10	9.97	(25.32)	4.76	(0.121)	824
S-11	9.97	(25.32)	4.31	(0.109)	925
S-12	9.97	(25.32)	5.02	(0.128)	797
S-13	9.97	(25.32)	5.48	(0.139)	730
S-14	9.97	(25.32)	5.04	(0.128)	795
S-15	9.97	(25.32)	5.12	(0.130)	783
S-16	9.97	(25.32)	3.97	(0.101)	1000

TABLE II

THICKNESS VARIATION OF SHELLS

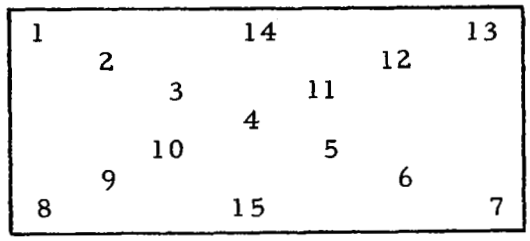

Numbers indicate position on shell at which thickness specimens were cut.

Thickness inches x 10^3 (mm)

Position	Shell S-8		Shell S-11		Shell S-12	
1	4.82	(0.122)	4.31	(0.109)	5.00	(0.127)
2	4.87	(0.124)	4.36	(0.111)	4.88	(0.124)
3	4.88	(0.124)	4.40	(0.112)	4.85	(0.123)
4	4.80	(0.122)	4.39	(0.112)	4.94	(0.125)
5	4.72	(0.120)	4.34	(0.110)	5.05	(0.128)
6	4.66	(0.118)	4.26	(0.108)	5.17	(0.131)
7	4.65	(0.118)	4.19	(0.106)	5.21	(0.132)
8	4.88	(0.124)	4.26	(0.108)	4.89	(0.124)
9	4.89	(0.124)	4.34	(0.110)	4.81	(0.122)
10	4.85	(0.123)	4.40	(0.112)	4.82	(0.122)
11	4.74	(0.120)	4.35	(0.110)	4.97	(0.126)
12	4.69	(0.119)	4.28	(0.109)	5.17	(0.131)
13	4.68	(0.119)	4.23	(0.107)	5.17	(0.131)
14	4.81	(0.122)	4.39	(0.112)	4.98	(0.126)
15	4.77	(0.121)	4.41	(0.112)	4.92	(0.125)
Average	4.78	(0.121)	4.33	(0.110)	4.99	(0.127)

TABLE III

YOUNG'S MODULUS TEST RESULTS

Shell	E		$\frac{E_{max} - E_{min}}{E_{ave}}$ %
	psi x 10^{-6}	(GN/m^2)	
S-1	15.3	(105.5)	9.2
S-2	16.7	(115.1)	2.0
S-3	15.1	(104.1)	12.0
S-4	15.0	(103.4)	6.6
S-5	15.3	(105.5)	4.6
S-6	15.7	(109.2)	5.2
S-7	14.9	(102.7)	8.0
S-8	16.0	(110.3)	5.0
S-9	16.8	(115.8)	7.2
S-10	15.9	(109.6)	9.4
S-11	16.0	(110.3)	7.6
S-12	16.5	(113.8)	2.4
S-13	15.8	(108.9)	9.4
S-14	15.6	(107.6)	11.6
S-15	15.8	(108.9)	5.0
S-16	14.9	(102.7)	9.4

TABLE IV

RESULTS OF FOURIER ANALYSIS*

Strain gage reading = $A_o + B_n \cos(\theta - \zeta_n)$; n = 1, 2 . . .

Shell	A_o	B_1	ζ_1	B_2	ζ_2	B_3	ζ_3	B_4	ζ_4	B_5	ζ_5	B_6	ζ_6
S-1	145.4	96.8	-24°	9.6	-26°	2.5	-66°	0.8	-81°	3.9	2°	0.4	0°
S-2	340.1	6.5	10°	8.9	31°	9.3	-86°	5.3	-31°	3.4	-69°	1.9	0°
S-3	264.4	63.5	-35°	10.9	58°	8.6	-80°	3.2	-45°	1.9	64°	0.2	0°
S-4	209.9	145.6	-25°	13.9	25°	4.0	75°	2.2	68°	2.2	-88°	2.1	0°
S-5	282.7	44.4	-19°	11.2	-59°	7.5	-37°	3.4	40°	1.5	-22°	2.9	0°
S-6	111.7	204	-30°	16.8	-77°	4.4	24°	2.4	-79°	1.8	48°	0.5	0°
S-7	108.1	249.7	-32°	19.6	-67°	3.8	23°	2.4	-37°	3.0	-19°	0.7	0°
S-8	268.3	118.8	-34°	18.6	51°	9.1	55°	3.6	-45°	0.9	-46°	1.2	0°
S-9	213.0	150.1	-29°	9.3	-67°	11.5	- 4°	14.2	73°	5.4	-72°	5.3	0°
S-10	165.0	232.2	-33°	28.4	77°	6.1	69°	5.0	-31°	3.0	-82°	0.2	0°

TABLE IV (cont'd)

RESULTS OF FOURIER ANALYSIS

Strain gage reading = $A_o + B_n \cos(\theta - \zeta_n)$; n = 1, 2 . . .

Shell	A_o	B_1	ζ_1	B_2	ζ_2	B_3	ζ_3	B_4	ζ_4	B_5	ζ_5	B_6	ζ_6
S-11	51.6	307.3	-28°	29.9	-59°	4.1	-87°	15.3	82°	5.4	88°	1.6	0°
S-12	331.3	125.9	-17°	10.8	22°	16.2	18°	7.7	-69°	6.6	- 5°	0.2	0°
S-13	169.1	297.4	-35°	39.1	-88°	4.7	-75°	6.6	40°	7.9	-29°	1.3	0°
S-14	202.6	209.8	-25°	11.9	3°	6.6	72°	5.9	-76°	2.7	85°	2.5	0°
S-15	380.8	16.5	6°	10.5	-35°	9.4	-69°	2.8	- 4°	3.1	-25°	0.4	0°
S-16	25.7	263.0	-31°	10.0	-71°	4.4	59°	2.8	58°	1.9	54°	2.6	0°

* Tabulated values are strain gage readings in mv x 10^2 at buckling.

TABLE V

SUMMARY OF BUCKLING DATA

Shell	$\sigma_{b\ max}$ psi	$\sigma_{b\ max}$ (MN/m^2)	$\sigma_{c\ max}$ psi	$\sigma_{c\ max}$ (MN/m^2)	C_c	$\frac{C_c}{C_{\bar{\sigma}}}$	C_b	$\frac{C_b}{C_{\bar{\sigma}}}$
S-1	2456	(16.93)	3332	(22.97)	0.187	0.309	0.134	0.218
S-2	168	(1.16)	7945	(54.77)	0.417	0.690	0.01	0.016
S-3	1551	(10.69)	5828	(40.18)	0.319	0.527	0.083	0.137
S-4	3695	(25.47)	4811	(33.17)	0.274	0.453	0.205	0.239
S-5	1150	(7.93)	6618	(45.62)	0.38	0.628	0.064	0.106
S-6	5040	(34.75)	2492	(17.18)	0.133	0.220	0.261	0.481
S-7	6586	(45.40)	2575	(17.75)	0.154	0.254	0.384	0.635
S-8	3015	(20.79)	6150	(42.40)	0.33	0.545	0.158	0.261
S-9	3755	(26.03)	4811	(33.17)	0.243	0.401	0.184	0.304
S-10	5920	(40.81)	3798	(26.18)	0.206	0.341	0.313	0.517
S-11	8650	(59.63)	1310	(9.03)	0.078	0.129	0.501	0.829
S-12	3042	(20.97)	7230	(49.84)	0.367	0.606	0.150	0.248
S-13	6586	(45.40)	3380	(23.30)	0.160	0.264	0.304	0.502
S-14	5052	(34.83)	4403	(30.35)	0.23	0.380	0.257	0.425
S-15	391	(2.70)	8148	(56.17)	0.414	0.684	0.019	0.031
S-16	8038	(55.41)	708	(4.88)	0.049	0.081	0.543	0.897

TABLE VI

MYLAR SPECIMEN DETAILS

All Specimens - Radius = 4.0 in. (10.16 cm) Length = 10.0 in. (25.4 cm)

$E = E_{sheet} = 731,000$ psi $(5.04\ GN/m^2)$

Spec. No.	Sheet Thickness t in. (mm)	Seam Width w_s in. (mm)	Seam Thickness t_s in. (mm)	Seam Modulus E_s psi x 10^{-3} (GN/m^2)	E/E_s	Effective Area A_e $in.^2$ (mm^2)	Effective Mom. - Iner. I_e $in.^4$ $(mm^4 \times 10^{-4})$	Calculated c.g. offset e_o in. (mm)	Exper. c.g. offset e^*_o in. (mm)	Buckling Stress σ_c psi (MN/m^2)
1	0.0103 (0.262)	1.0 (25.4)	0.0252 (0.640)	605 (4.22)	0.828	0.2692 (173.7)	2.231 (92.86)	0.1560 (3.962)	0.150 (3.810)	1129 (7.784)
2	0.0103 (0.262)	0.5 (12.7)	0.0245 (0.622)	605 (4.22)	0.828	0.2636 (170.1)	2.162 (89.99)	0.0758 (1.925)	0 (0)	1129 (7.784)
3	0.0103 (0.262)	0.2 (5.08)	0.0258 (0.655)	605 (4.22)	0.828	0.2609 (168.3)	2.105 (87.62)	0.0340 (0.864)	-0.030 (-0.762)	1129 (7.784)
4	0.00718 (0.182)	1.0 (25.4)	0.0210 (0.533)	605 (4.22)	0.828	0.1909 (123.2)	1.597 (66.47)	0.2141 (5.438)	0.300 (7.620)	786 (5.419)
5	0.00718 (0.182)	0.5 (12.7)	0.0186 (0.472)	605 (4.22)	0.828	0.1848 (119.2)	1.507 (62.73)	0.0890 (2.261)	0.030 (0.762)	786 (5.419)
6	0.00718 (0.182)	0.2 (5.08)	0.0225 (0.572)	605 (4.22)	0.828	0.1830 (118.1)	1.478 (61.52)	0.0500 (1.270)	0 (0)	786 (5.419)
7	0.00475 (0.121)	1.0 (25.4)	0.0160 (0.406)	530 (3.70)	0.725	0.1245 (80.3)	1.046 (43.54)	0.1860 (4.724)	0.250 (6.350	520 (3.585)

TABLE VII

MYLAR TEST RESULTS

Load* Point	Specimen No. 1			Specimen No. 2			Specimen No. 3		
	$\frac{\sigma_c}{\sigma_{c\ell}}$	$\frac{\sigma_b}{\sigma_{c\ell}}$	$\frac{\sigma_t}{\sigma_{c\ell}}$	$\frac{\sigma_c}{\sigma_{c\ell}}$	$\frac{\sigma_b}{\sigma_{c\ell}}$	$\frac{\sigma_t}{\sigma_{c\ell}}$	$\frac{\sigma_c}{\sigma_{c\ell}}$	$\frac{\sigma_b}{\sigma_{c\ell}}$	$\frac{\sigma_t}{\sigma_{c\ell}}$
1	0.297	0.569	0.866	0.296	0.550	0.846	0.259	0.483	0.742
2	0.321	0.542	0.863	0.312	0.508	0.820	0.284	0.464	0.748
3	0.344	0.503	0.847	0.351	0.494	0.845	0.308	0.432	0.740
4	0.383	0.472	0.855	0.383	0.450	0.833	0.340	0.399	0.739
5	0.422	0.424	0.846	0.415	0.391	0.806	0.373	0.349	0.721
6	0.445	0.395	0.840	0.447	0.369	0.816	0.396	0.326	0.722
7	0.468	0.362	0.830	0.470	0.334	0.804	0.428	0.302	0.730
8	0.499	0.328	0.837	0.510	0.302	0.812	0.468	0.274	0.742
9	0.538	0.291	0.829	0.550	0.261	0.811	0.500	0.234	0.734
10	0.569	0.241	0.810	0.565	0.202	0.767	0.540	0.188	0.728
11	0.608	0.186	0.794	0.621	0.148	0.769	0.588	0.148	0.736
12	0.662	0.125	0.787	0.676	0.081	0.757	0.668	0.071	0.739
13	0.716	0.051	0.767	0.739	0	0.739	0.740	0.011	0.751
14	0.770	0.036	0.806	0.676	0.081	0.757	0.684	0.093	0.777
15	0.654	0.108	0.762	0.613	0.146	0.759	0.620	0.159	0.779

TABLE VII (Cont'd)

MYLAR TEST RESULTS

Load* Point	Specimen No. 1			Specimen No. 2			Specimen No. 3		
	$\frac{\sigma_c}{\sigma_{c\ell}}$	$\frac{\sigma_b}{\sigma_{c\ell}}$	$\frac{\sigma_t}{\sigma_{c\ell}}$	$\frac{\sigma_c}{\sigma_{c\ell}}$	$\frac{\sigma_b}{\sigma_{c\ell}}$	$\frac{\sigma_t}{\sigma_{c\ell}}$	$\frac{\sigma_c}{\sigma_{c\ell}}$	$\frac{\sigma_b}{\sigma_{c\ell}}$	$\frac{\sigma_t}{\sigma_{c\ell}}$
16	0.600	0.170	0.770	0.573	0.205	0.778	0.564	0.213	0.777
17	0.546	0.218	0.764	0.525	0.241	0.776	0.516	0.256	0.772
18	0.491	0.254	0.745	0.494	0.293	0.787	0.468	0.288	0.756
19	0.460	0.291	0.751	0.462	0.328	0.790	0.424	0.311	0.735
20	0.429	0.321	0.750	0.431	0.356	0.787	0.392	0.333	0.725
21	0.398	0.344	0.742	0.415	0.391	0.806	0.372	0.360	0.732
22	0.359	0.392	0.751	0.367	0.431	0.798	0.331	0.399	0.730
23	0.328	0.433	0.761	0.336	0.471	0.807	0.300	0.429	0.729
24	0.298	0.460	0.758	0.296	0.481	0.777	0.276	0.458	0.734
25	0.274	0.485	0.759	0.280	0.520	0.800	0.251	0.475	0.726

* Points 1 - 13 max bending stress is on side opposite seam.
Points 13 - 25 max bending stress is at the seam.

R/t for Specimens 1, 2 and 3 = 388.

TABLE VII (Cont'd)

MYLAR TEST RESULTS

Load*	Specimen No. 4			Specimen No. 5		
	$\frac{\sigma_c}{\sigma_{c\ell}}$	$\frac{\sigma_b}{\sigma_{c\ell}}$	$\frac{\sigma_t}{\sigma_{c\ell}}$	$\frac{\sigma_c}{\sigma_{c\ell}}$	$\frac{\sigma_b}{\sigma_{c\ell}}$	$\frac{\sigma_t}{\sigma_{c\ell}}$
1	0.298	0.554	0.852	0.265	0.470	0.735
2	0.322	0.532	0.854	0.285	0.445	0.730
3	0.353	0.512	0.865	0.298	0.402	0.700
4	0.369	0.456	0.825	0.346	0.396	0.742
5	0.417	0.426	0.843	0.395	0.366	0.761
6	0.432	0.395	0.827	0.411	0.335	0.746
7	0.464	0.374	0.838	0.447	0.315	0.762
8	0.480	0.334	0.814	0.476	0.282	0.758
9	0.511	0.299	0.810	0.525	0.251	0.776
10	0.535	0.254	0.789	0.557	0.203	0.760
11	0.606	0.220	0.826	0.606	0.150	0.756
12	0.637	0.160	0.797	0.671	0.088	0.759
13	0.669	0.092	0.761	0.703	0.010	0.713
14	0.763	0.018	0.781	0.661	0.068	0.729
15	0.732	0.067	0.799	0.590	0.129	0.719
16	0.669	0.137	0.806	0.525	0.176	0.701
17	0.621	0.198	0.819	0.492	0.221	0.713
18	0.590	0.254	0.844	0.460	0.259	0.719
19	0.558	0.303	0.861	0.428	0.288	0.716
20	0.519	0.339	0.858	0.395	0.310	0.706
21	0.495	0.379	0.874	0.379	0.340	0.719
22	0.432	0.424	0.856	0.334	0.370	0.705
23	0.401	0.480	0.881	0.301	0.398	0.699
24	0.353	0.497	0.850	0.282	0.432	0.714
25	0.339	0.546	0.885	0.257	0.447	0.704

R/t for Specimens 4, 5 and 6 = 557

TABLE VII (Cont'd)

MYLAR TEST RESULTS

Load*	Specimen No. 6			Specimen No. 7		
	$\frac{\sigma_c}{\sigma_{c\ell}}$	$\frac{\sigma_b}{\sigma_{c\ell}}$	$\frac{\sigma_t}{\sigma_{c\ell}}$	$\frac{\sigma_c}{\sigma_{c\ell}}$	$\frac{\sigma_b}{\sigma_{c\ell}}$	$\frac{\sigma_t}{\sigma_{c\ell}}$
1	0.286	0.508	0.794	0.212	0.381	0.593
2	0.318	0.501	0.819	0.230	0.369	0.599
3	0.351	0.481	0.832	0.248	0.346	0.594
4	0.384	0.439	0.823	0.273	0.328	0.601
5	0.416	0.383	0.799	0.295	0.292	0.587
6	0.433	0.350	0.783	0.320	0.283	0.603
7	0.466	0.324	0.790	0.338	0.263	0.601
8	0.498	0.290	0.788	0.356	0.239	0.595
9	0.531	0.248	0.779	0.403	0.227	0.630
10	0.556	0.196	0.752	0.417	0.189	0.606
11	0.613	0.145	0.758	0.446	0.152	0.598
12	0.646	0.076	0.722	0.490	0.112	0.602
13	0.728	0	0.728	0.536	0.062	0.598
14	0.679	0.080	0.759	0.591	0	0.591
15	0.605	0.142	0.747	0.536	0.062	0.598
16	0.564	0.198	0.762	0.482	0.110	0.592
17	0.548	0.257	0.805	0.454	0.154	0.608
18	0.482	0.280	0.762	0.418	0.188	0.606
19	0.457	0.318	0.775	0.392	0.220	0.612
20	0.425	0.343	0.768	0.374	0.252	0.626
21	0.400	0.368	0.768	0.356	0.278	0.634
22	0.368	0.419	0.787	0.309	0.307	0.616
23	0.335	0.454	0.789	0.302	0.366	0.668
24	0.302	0.473	0.775	0.266	0.376	0.642
25	0.286	0.508	0.794	0.248	0.401	0.649

R/t for Specimen No. 7 = 842

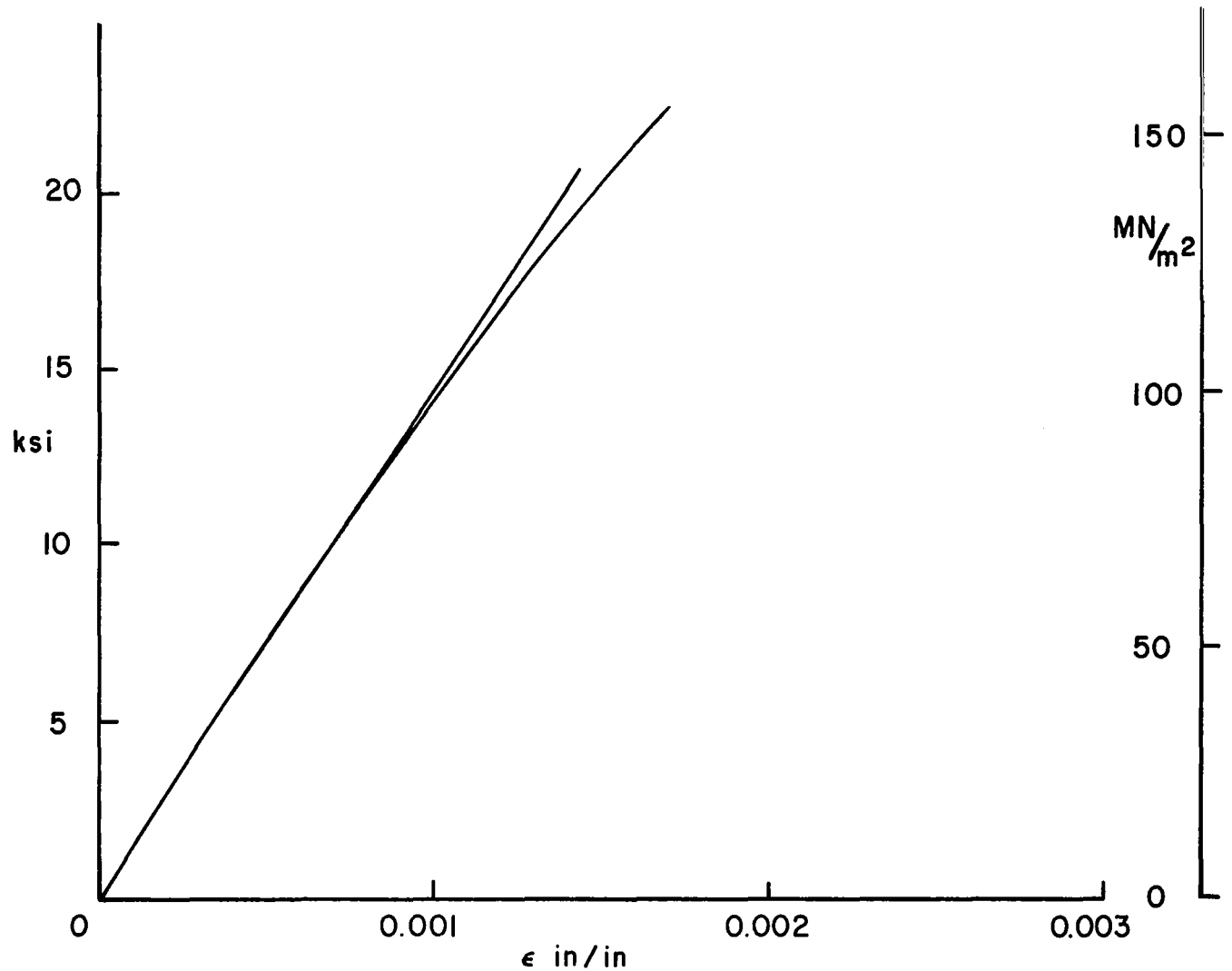

FIG. I TYPICAL STRESS STRAIN CURVE FOR PLATED COPPER

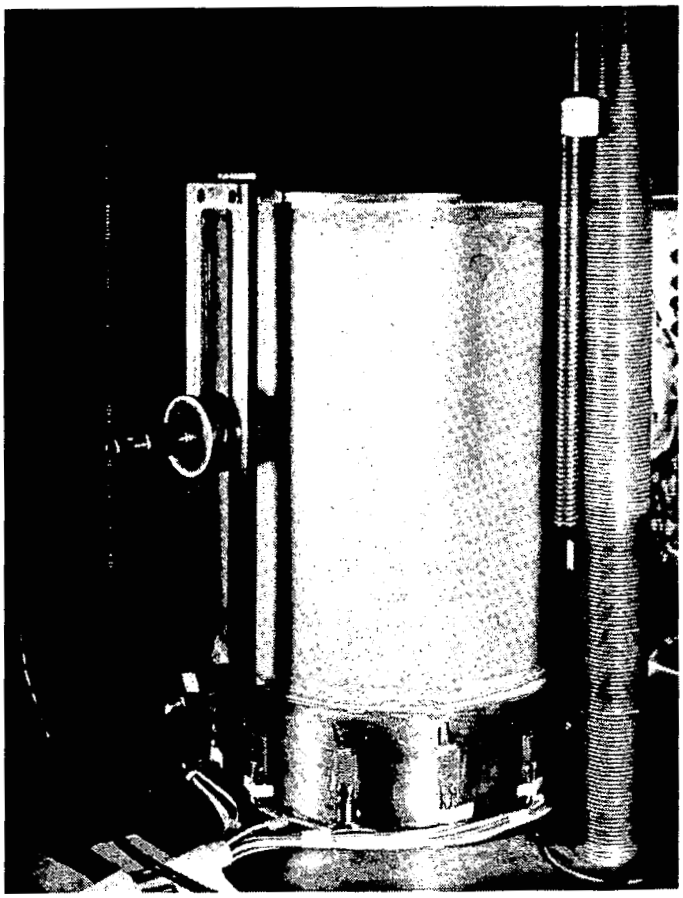

FIG. 2 SET UP FOR INITIAL IMPERFECTION MEASUREMENTS. PHOTOGRAPH COURTESY OF C. D. BABCOCK, JR.

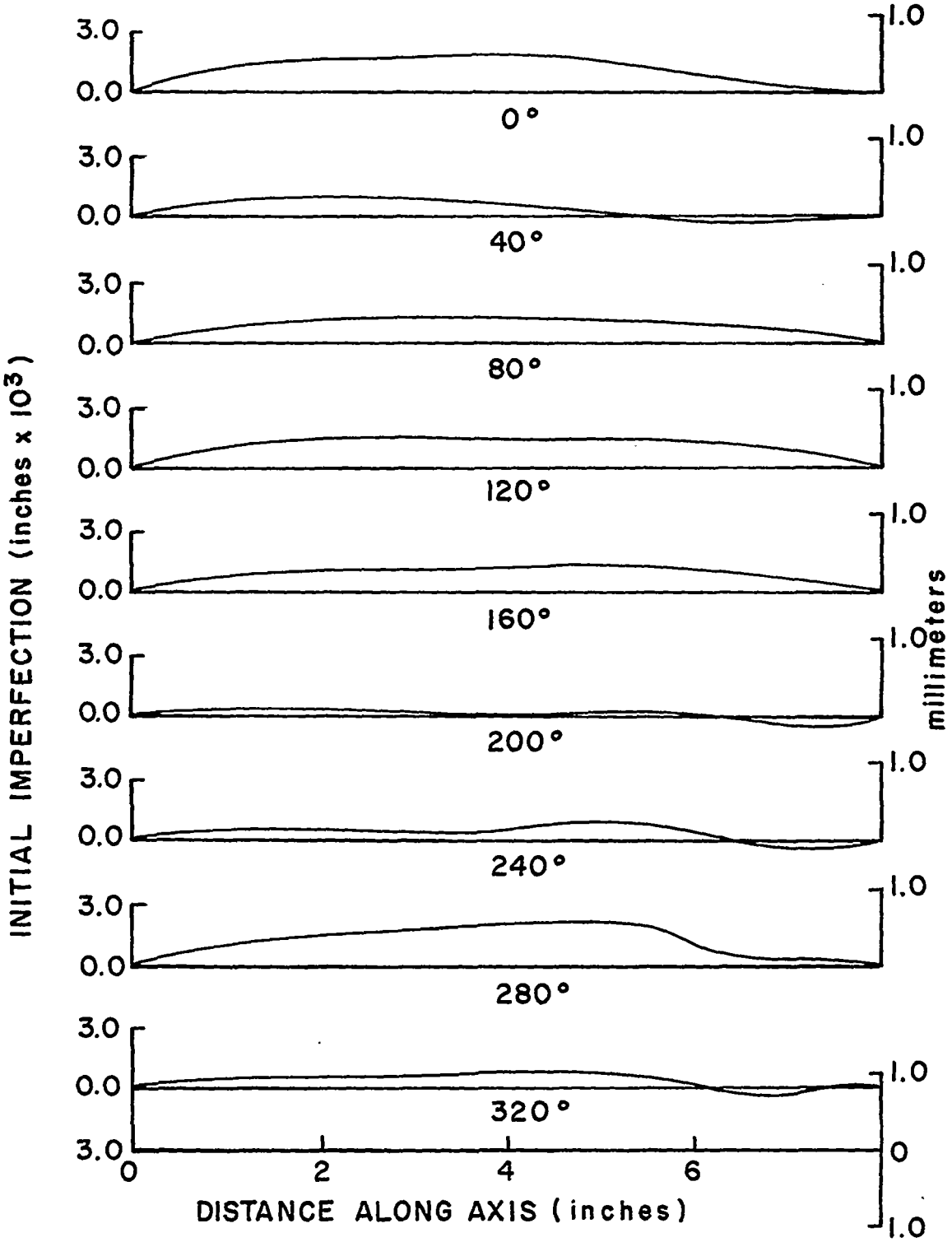

FIG. 3 INITIAL IMPERFECTION, SHELL SI

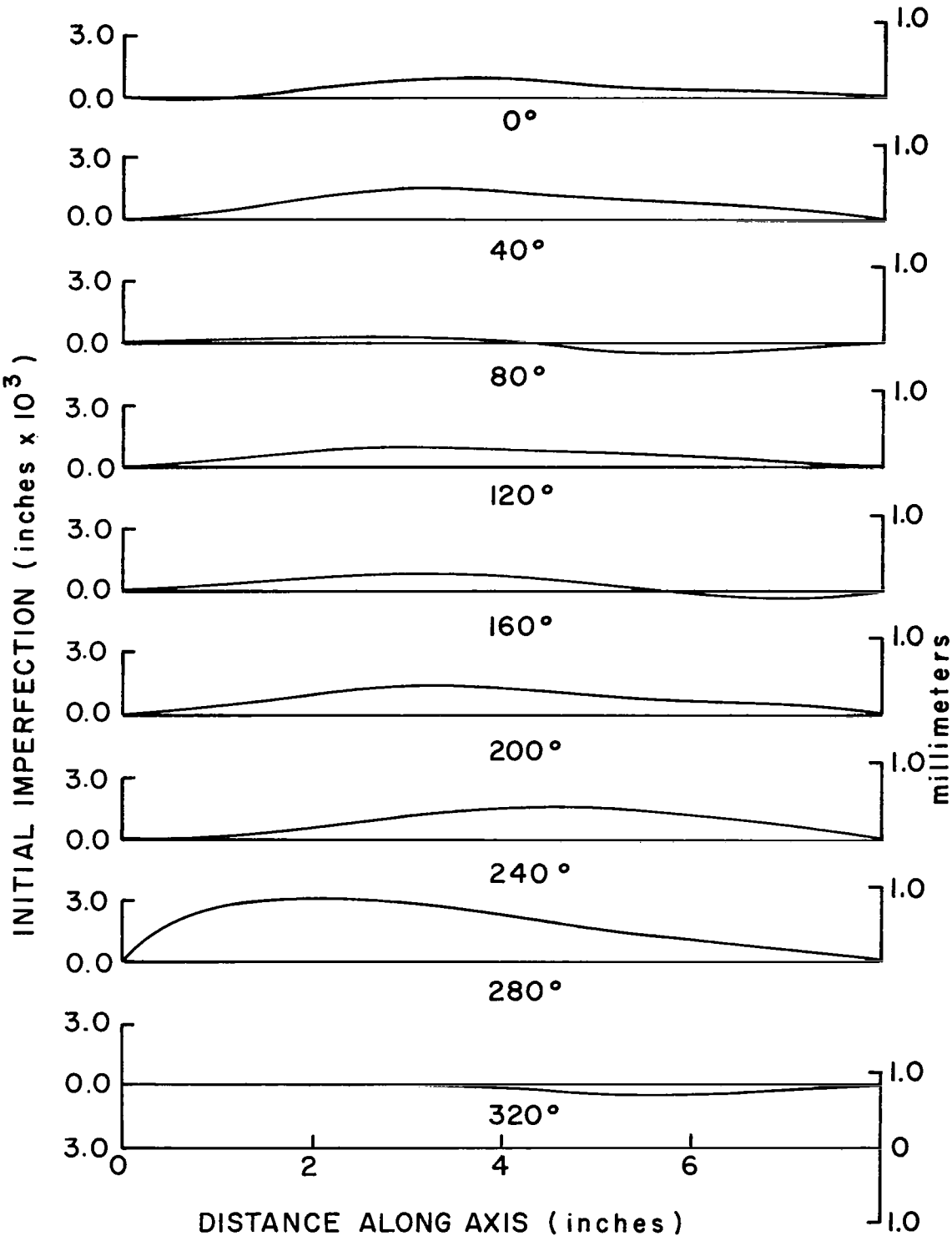

FIG. 4 INITIAL IMPERFECTION, SHELL S4

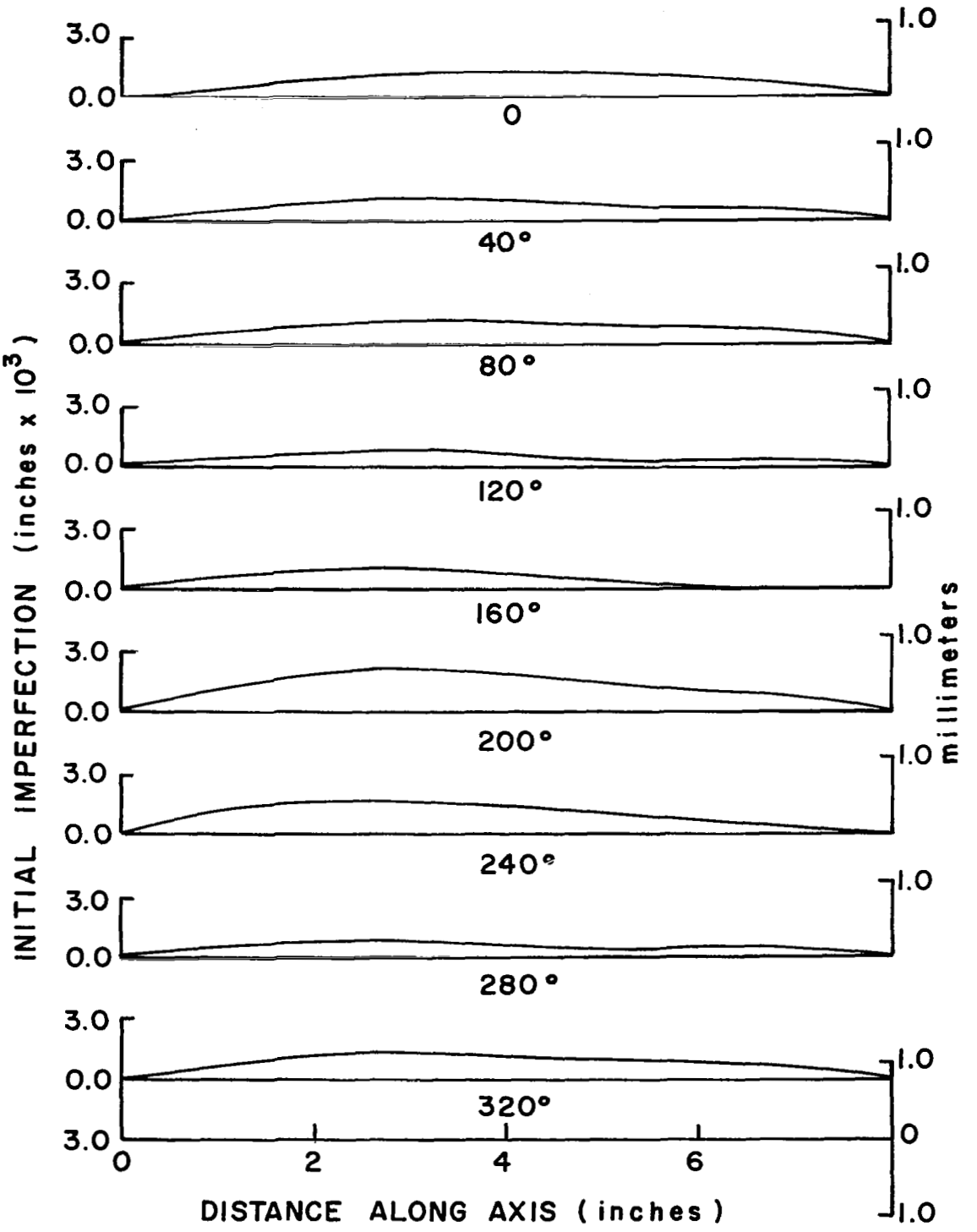

FIG. 5 INITIAL IMPERFECTION, SHELL S8

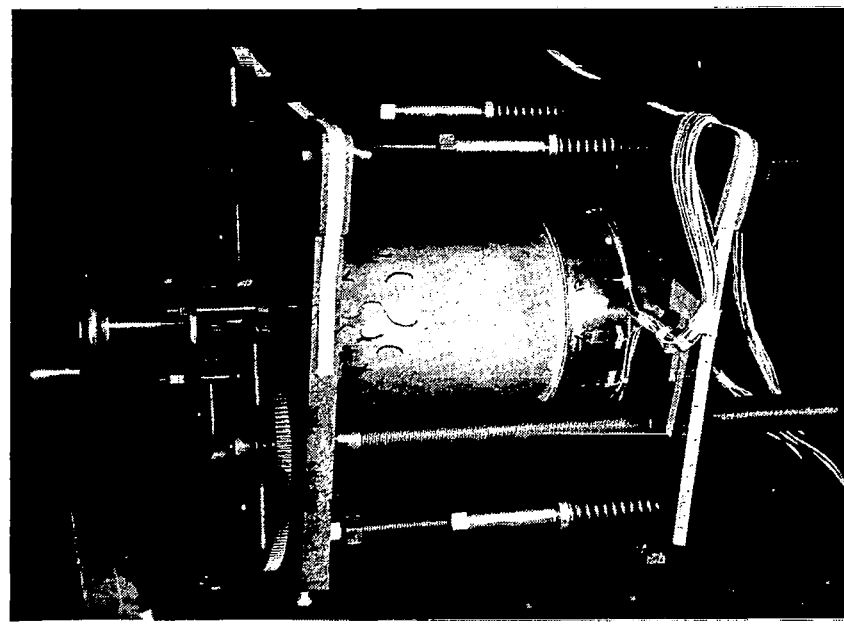

FIG. 6 TESTING MACHINE WITH SHELL IN TESTING POSITION. PHOTOGRAPH COURTESY OF C. D. BABCOCK, JR.

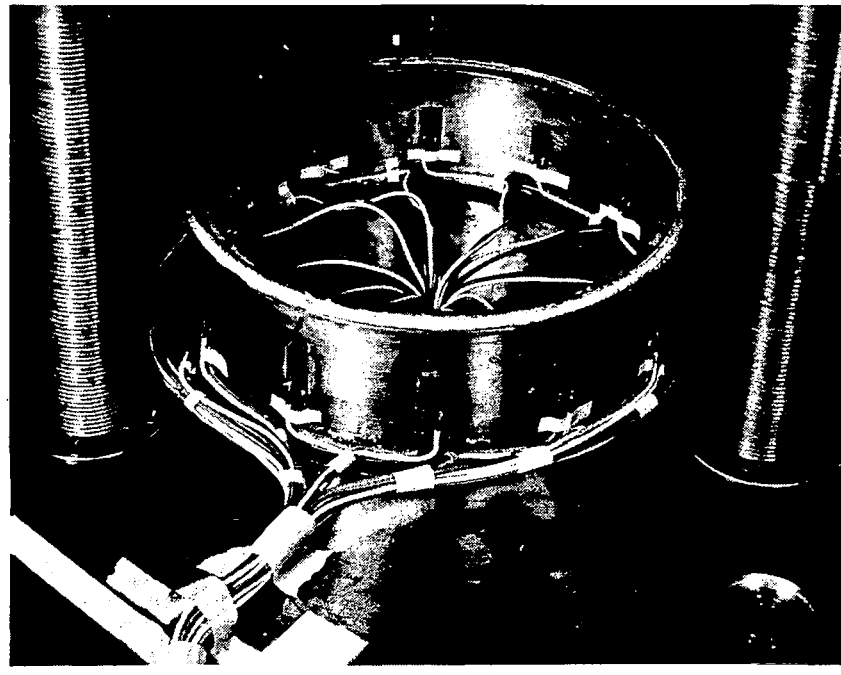

FIG. 7 LOAD MEASURING RING. PHOTOGRAPH COURTESY OF C. D. BABCOCK, JR.

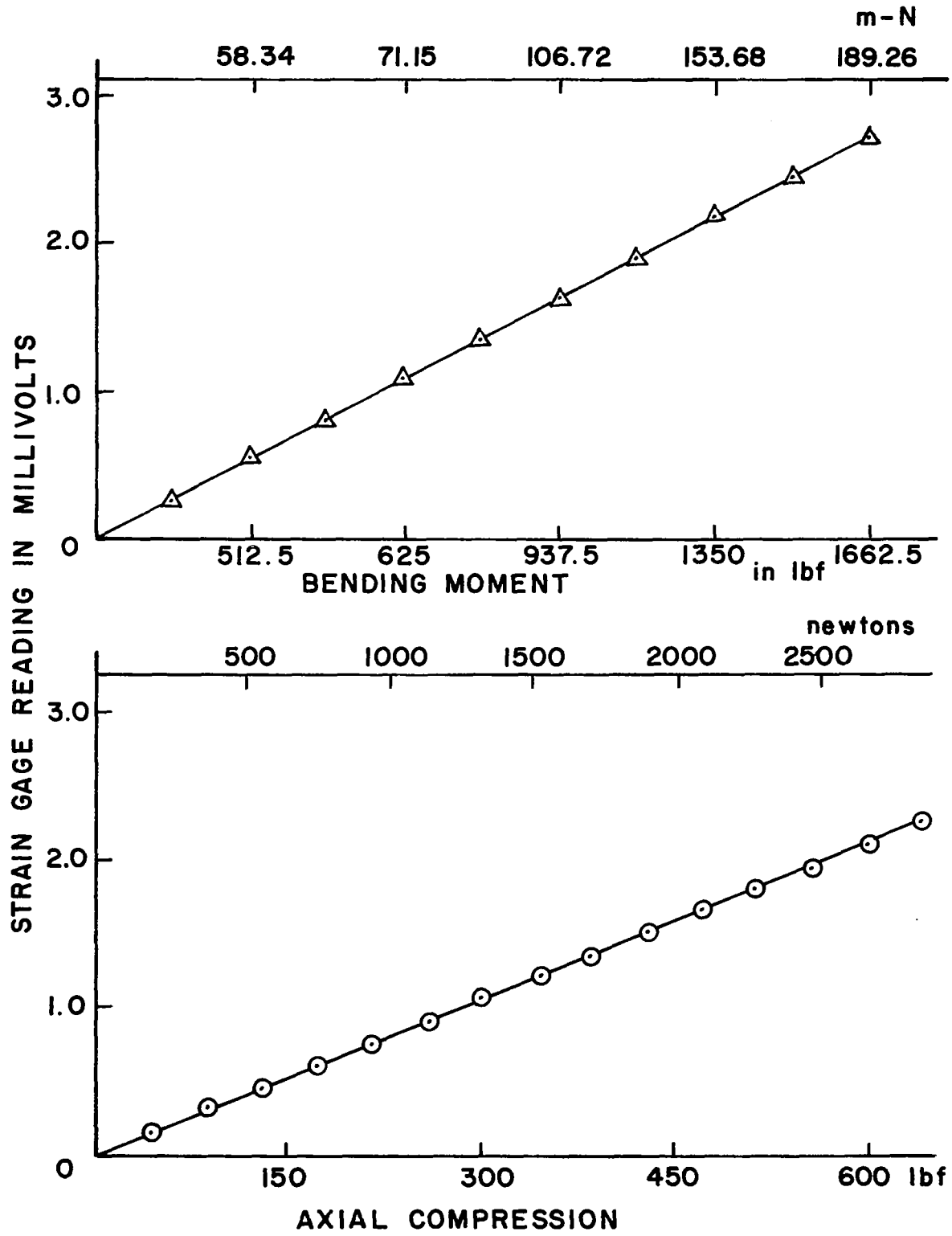

FIG. 8 LOAD RING CALIBRATION RESULTS

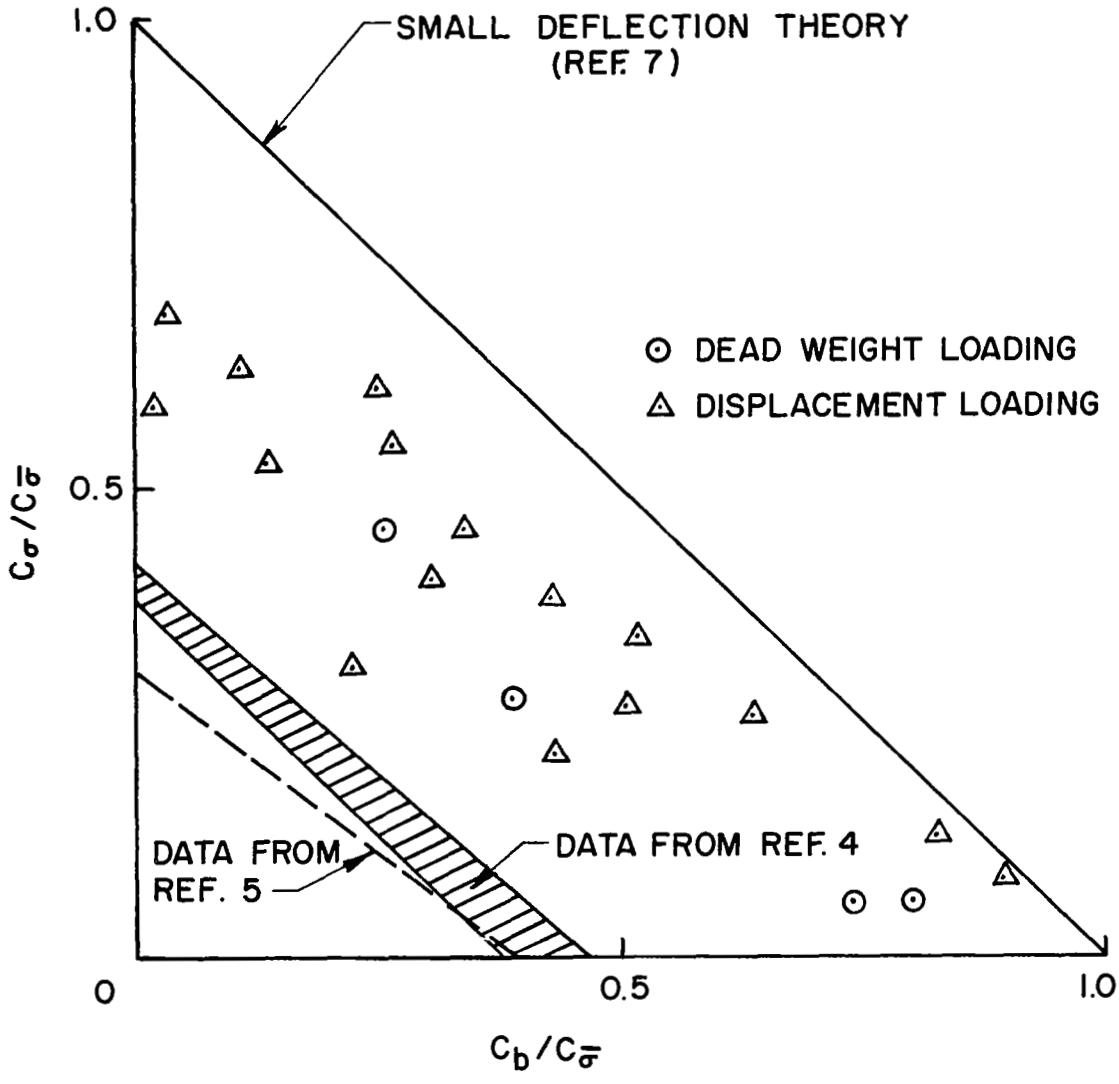

FIG. 9 INTERACTION CURVE, AXIAL COMPRESSION AND BENDING

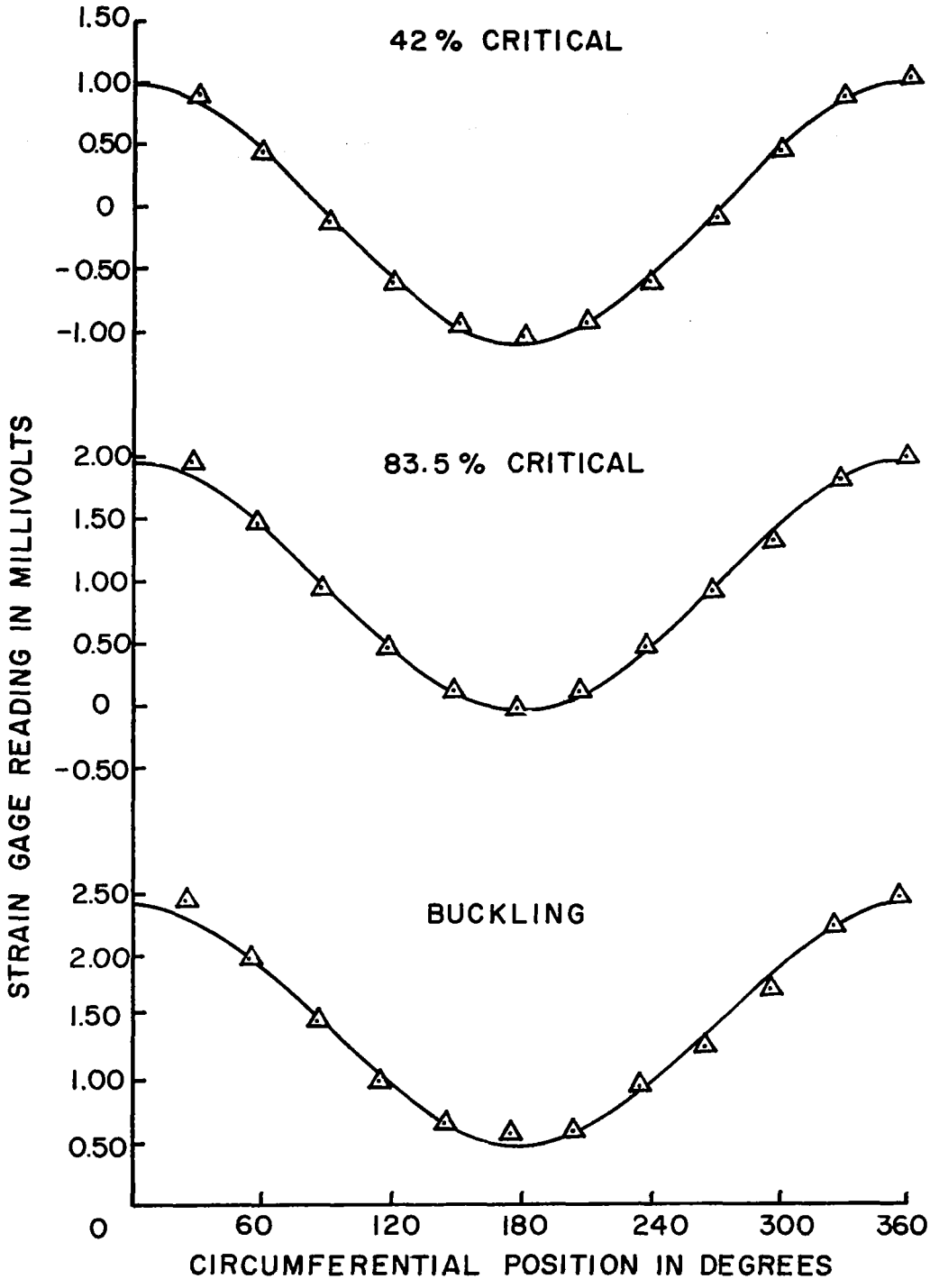

FIG. 10 COMPARISON OF COMPUTED LOAD DISTRIBUTION WITH STRAIN GAGE DATA FOR VARIOUS INCREMENTS OF LOADING ; SHELL S I

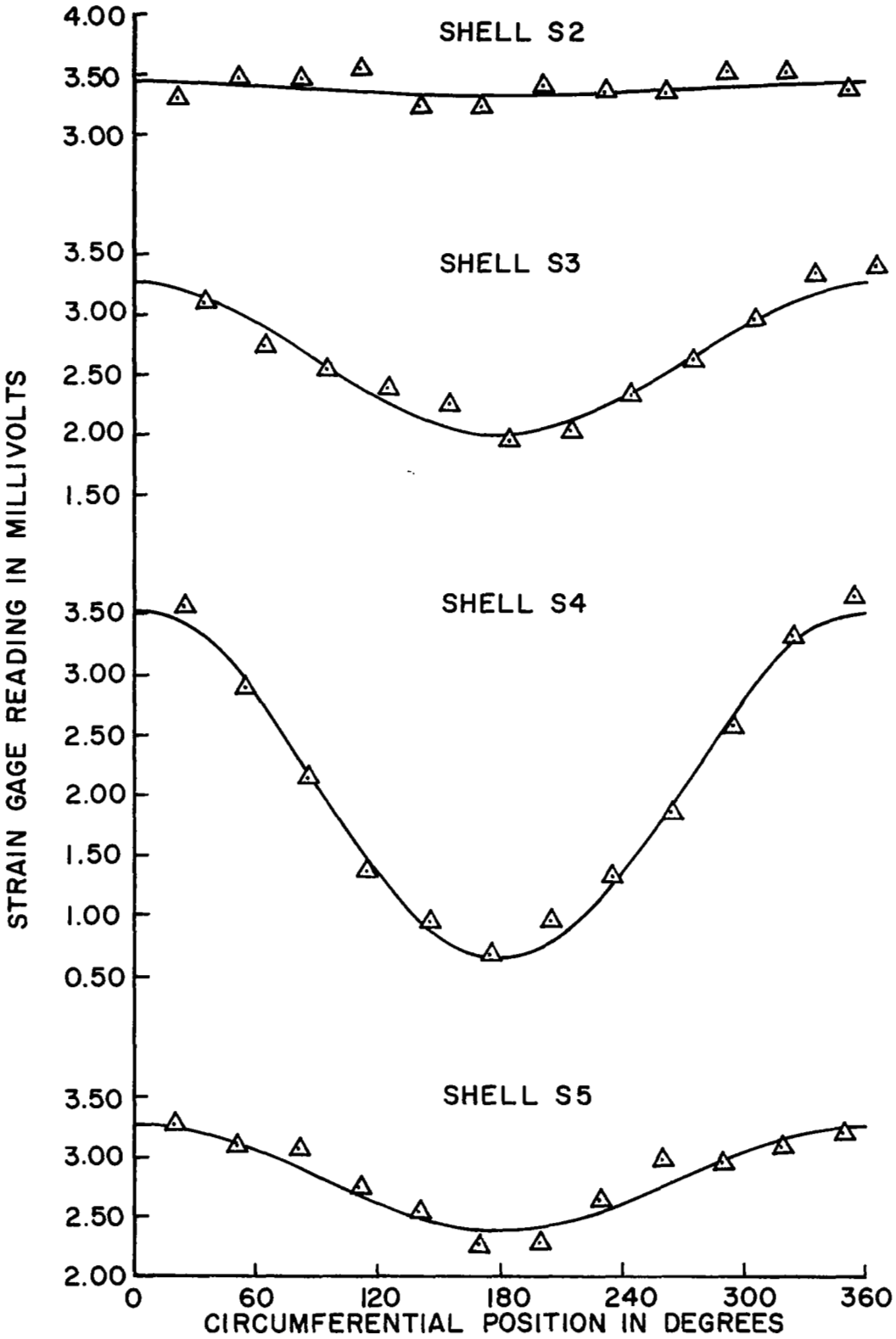

FIG. II COMPARISON OF COMPUTED LOAD DISTRIBUTION WITH STRAIN GAGE DATA AT BUCKLING, SHELLS S2,S3,S4,&S5

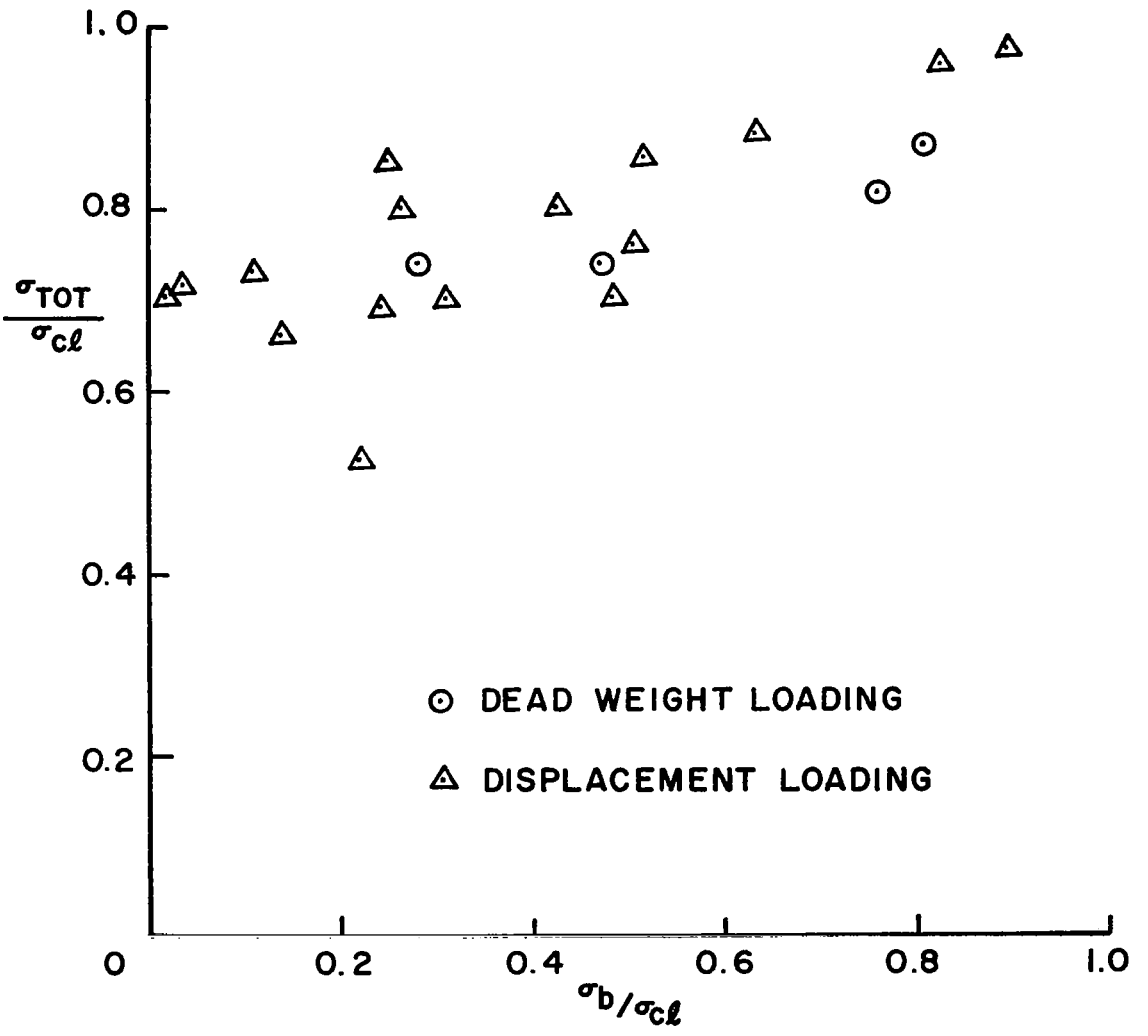

FIG. 12 INTERACTION CURVE FOR MAXIMUM TOTAL STRESS

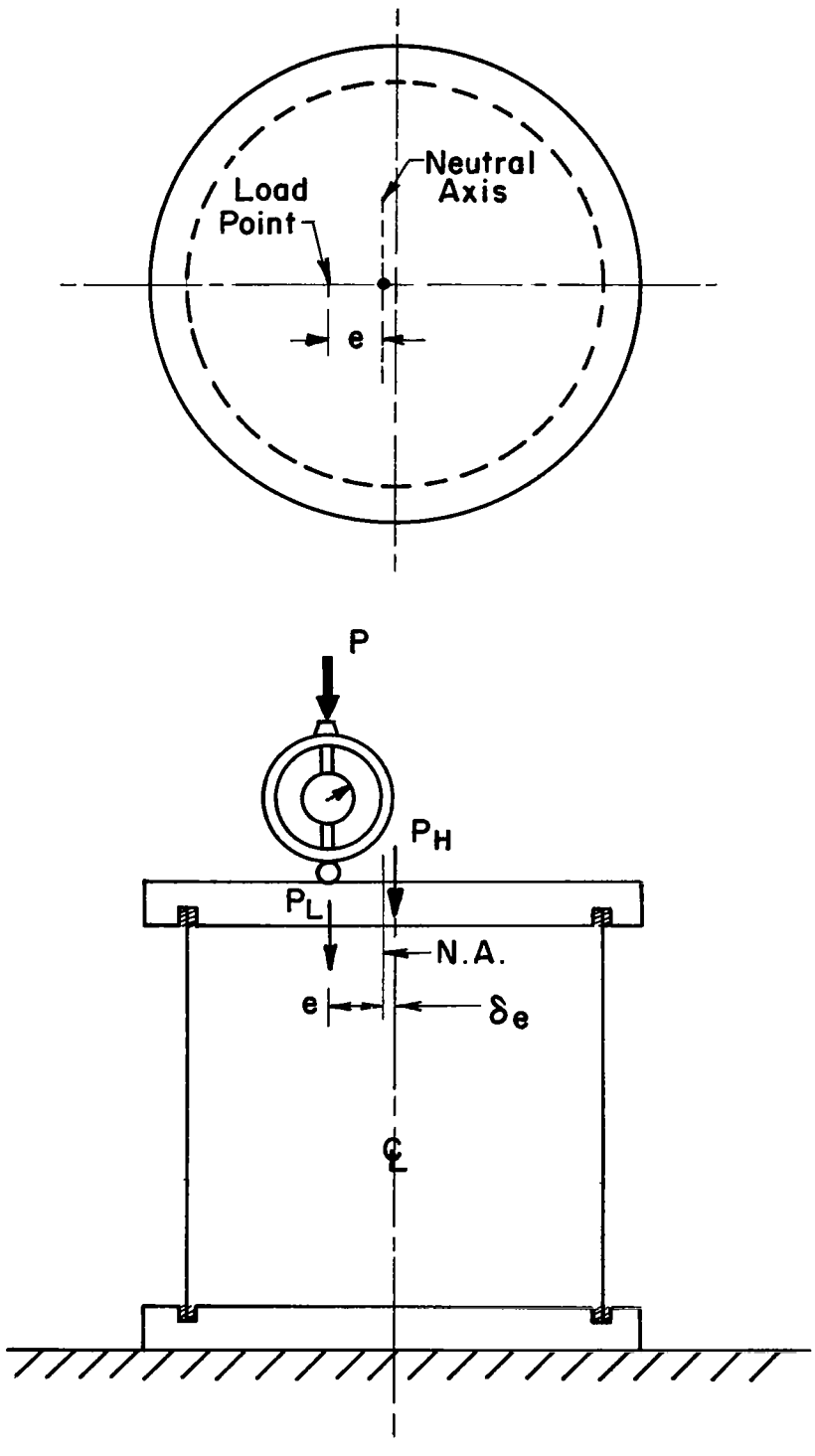

FIG. 13 MYLAR TEST SET – UP

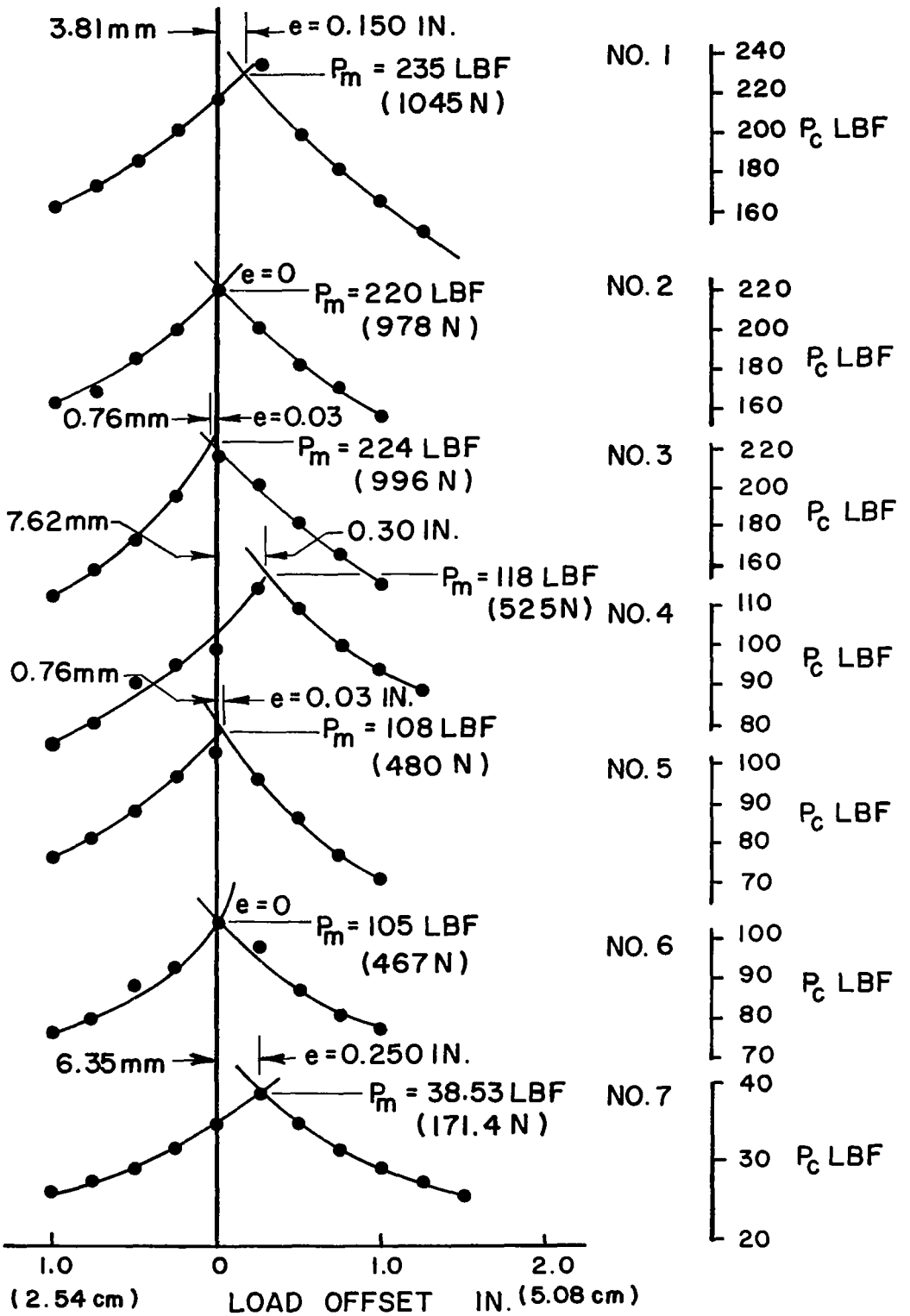

FIG. 14 DETERMINATION OF NEUTRAL AXIS

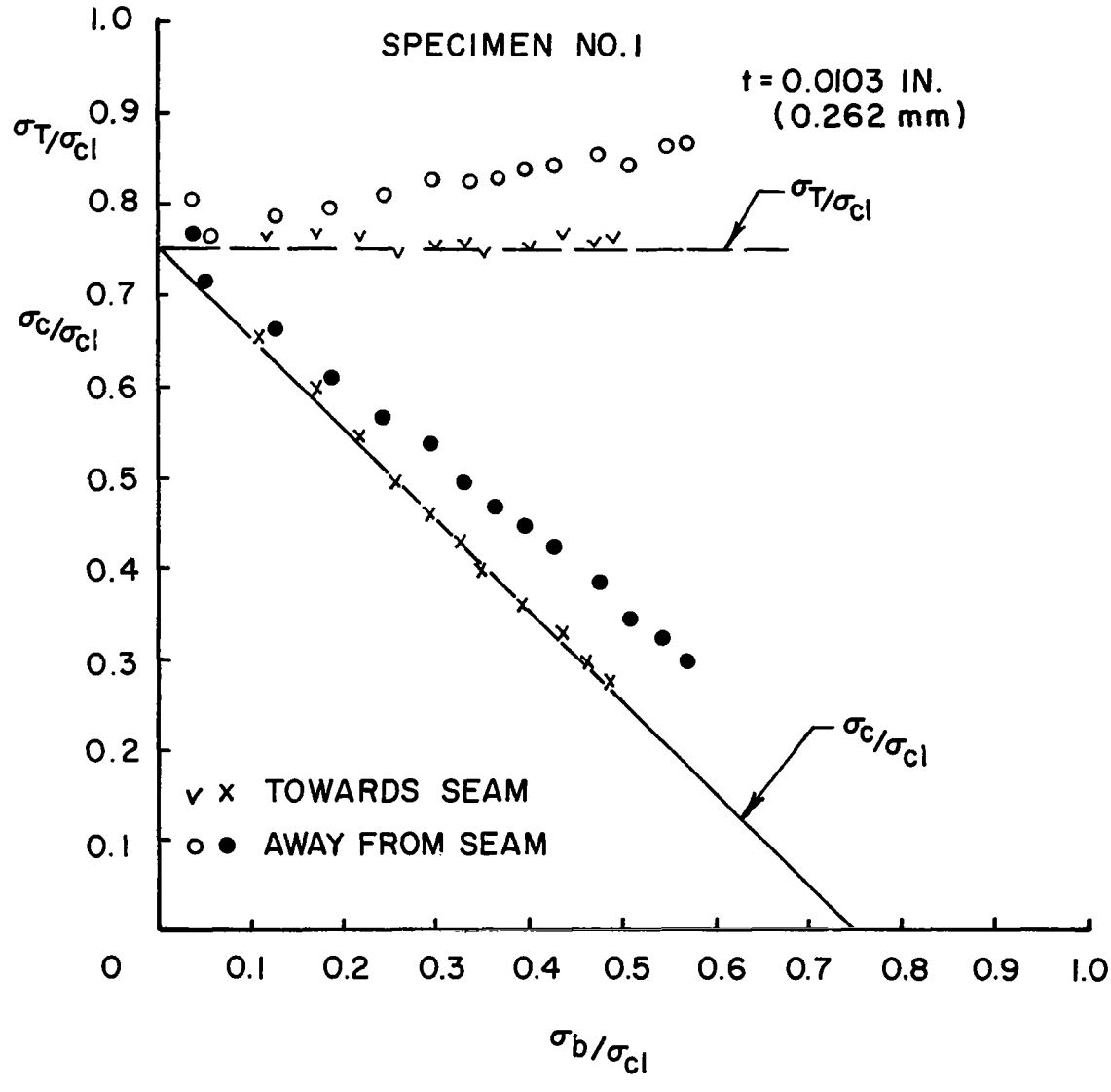

FIG. 15 INTERACTION CURVE

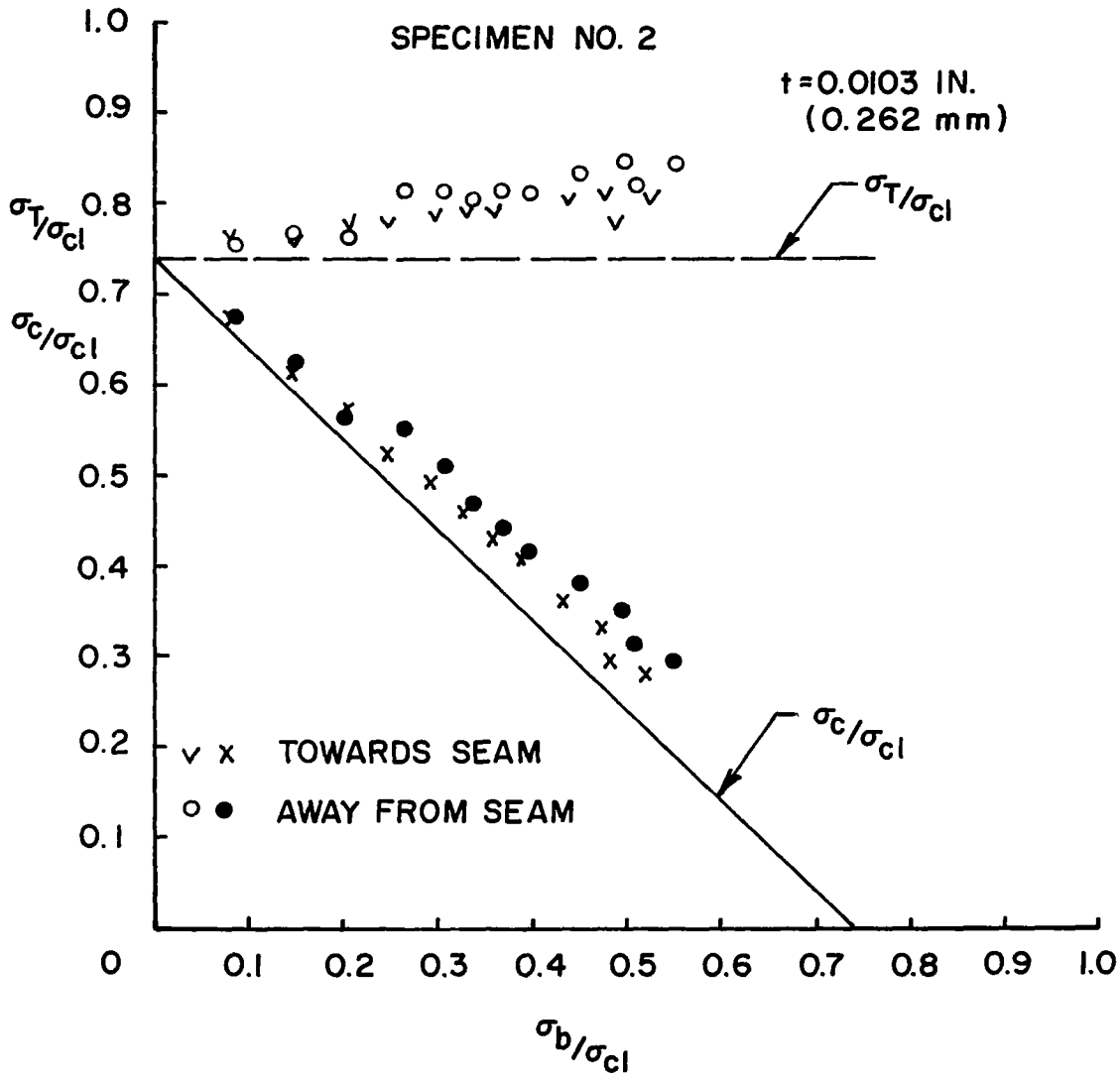

FIG. 16 INTERACTION CURVE

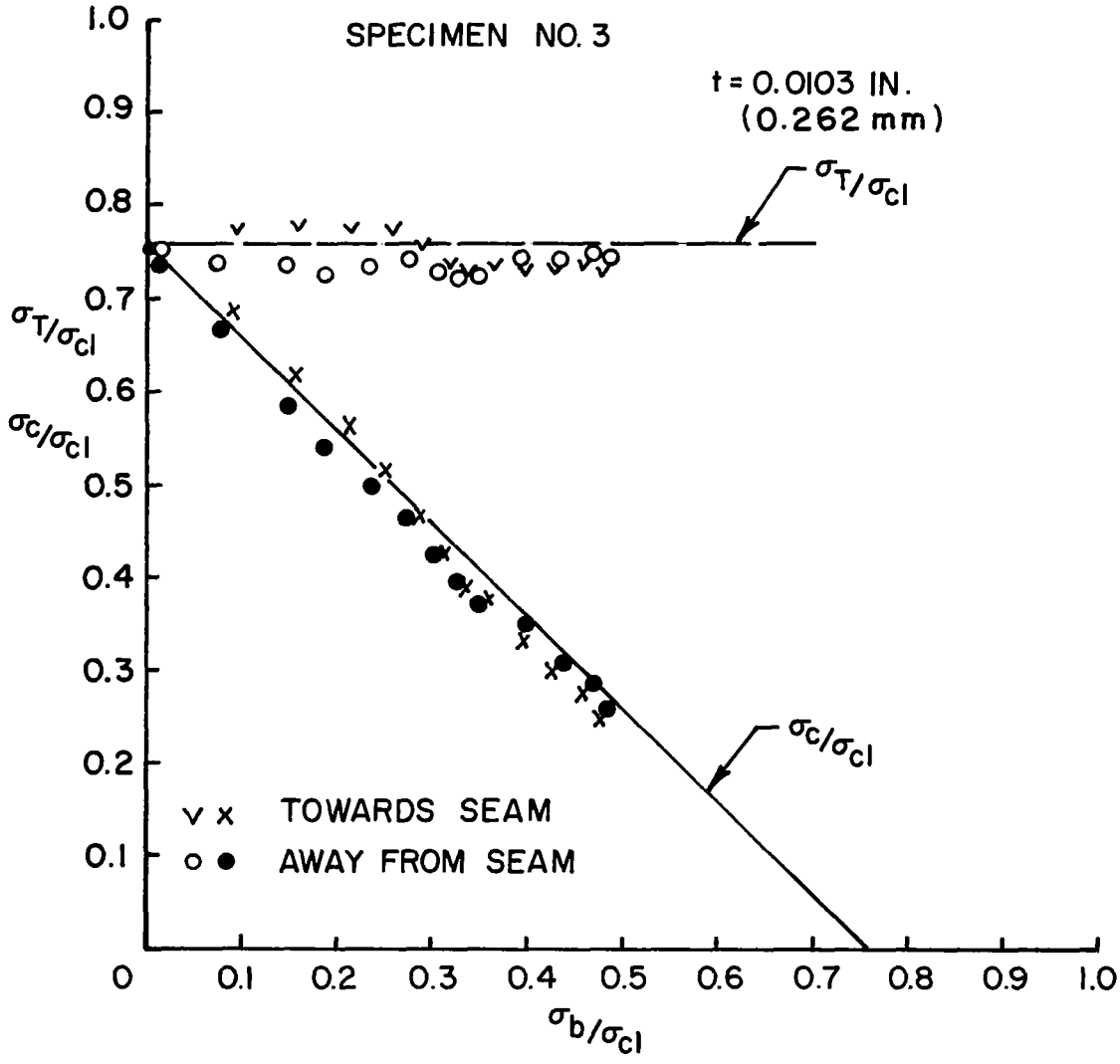

FIG. 17 INTERACTION CURVE

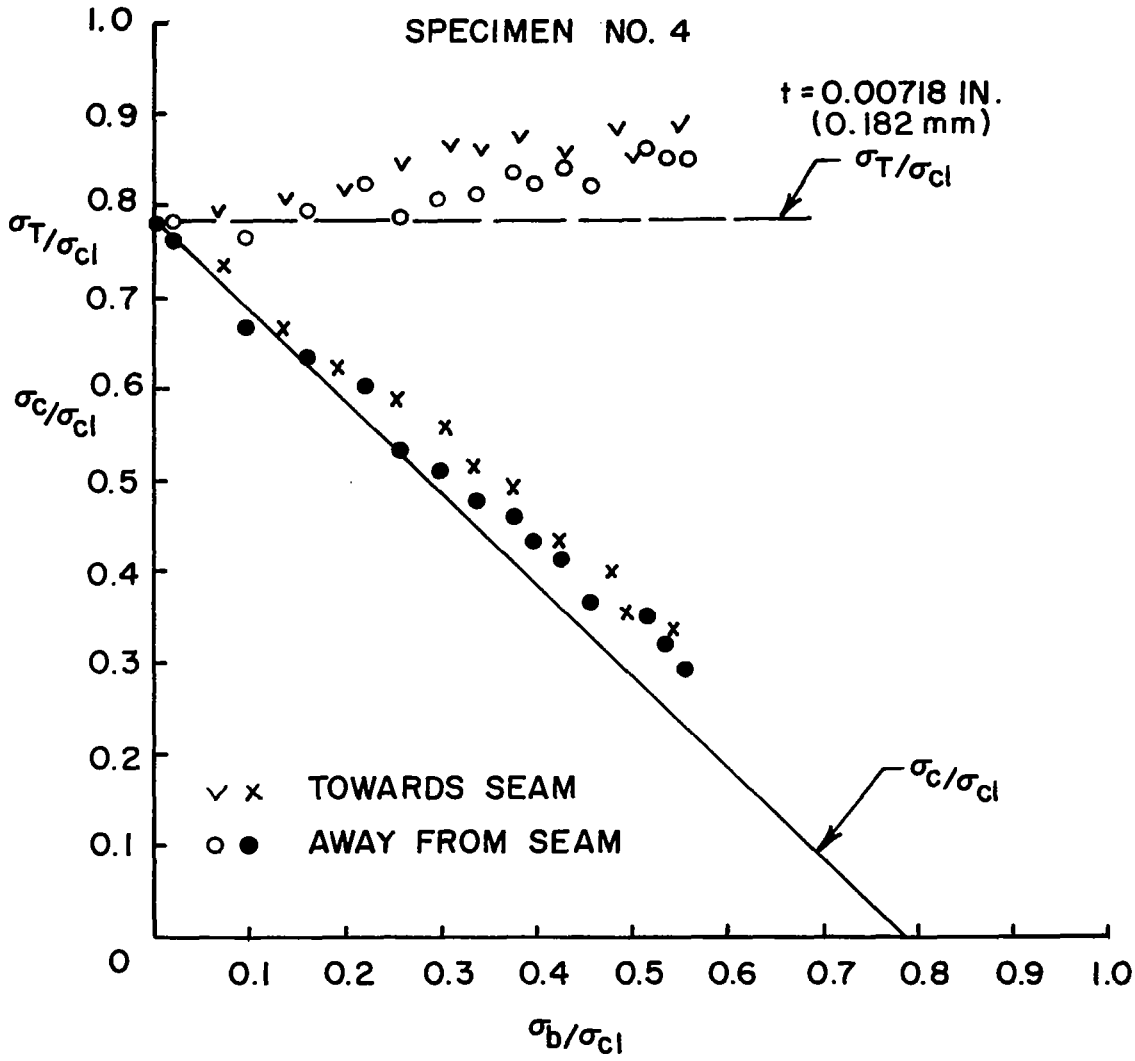

FIG. 18 INTERACTION CURVE

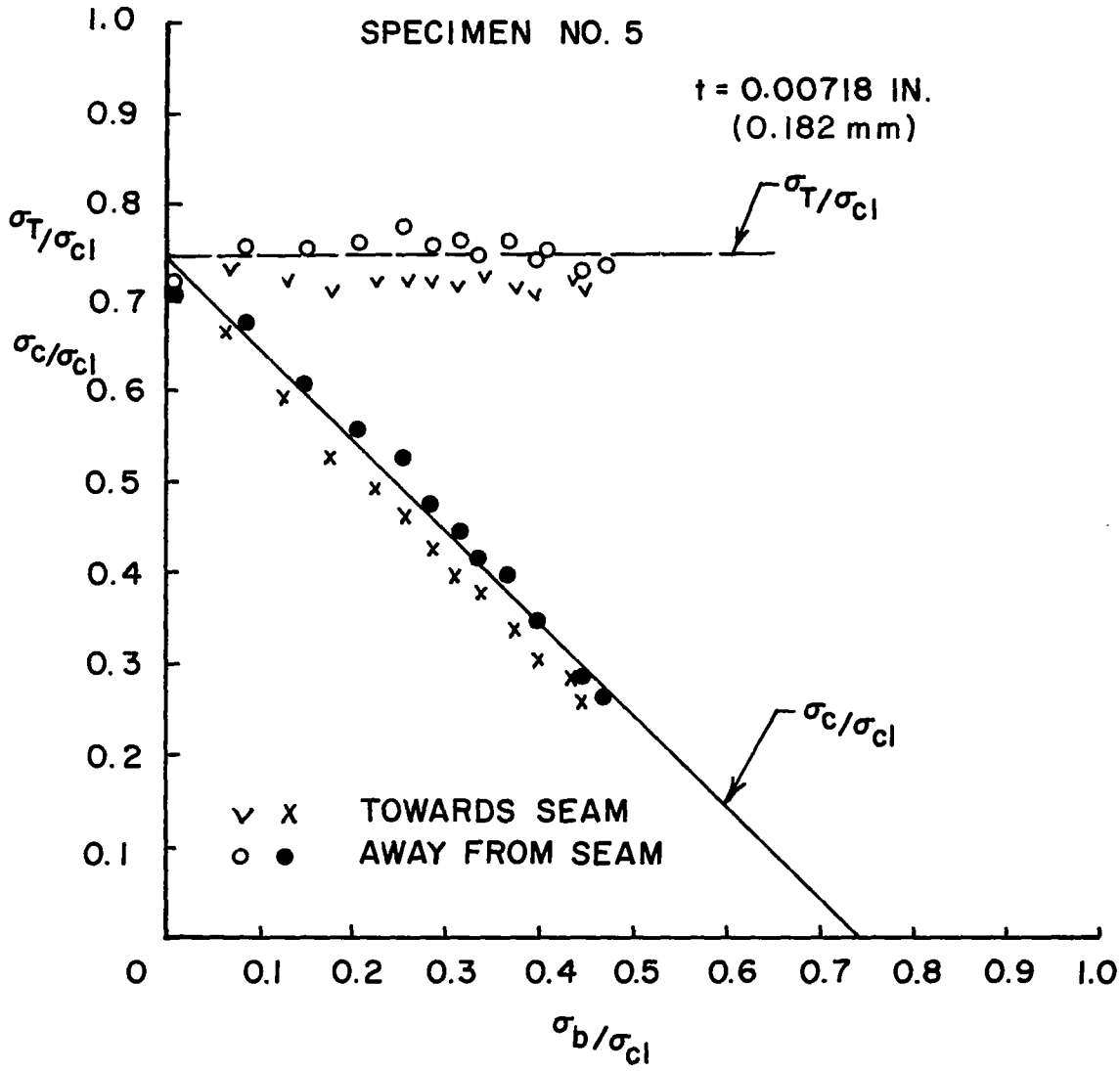

FIG. 19 INTERACTION CURVE

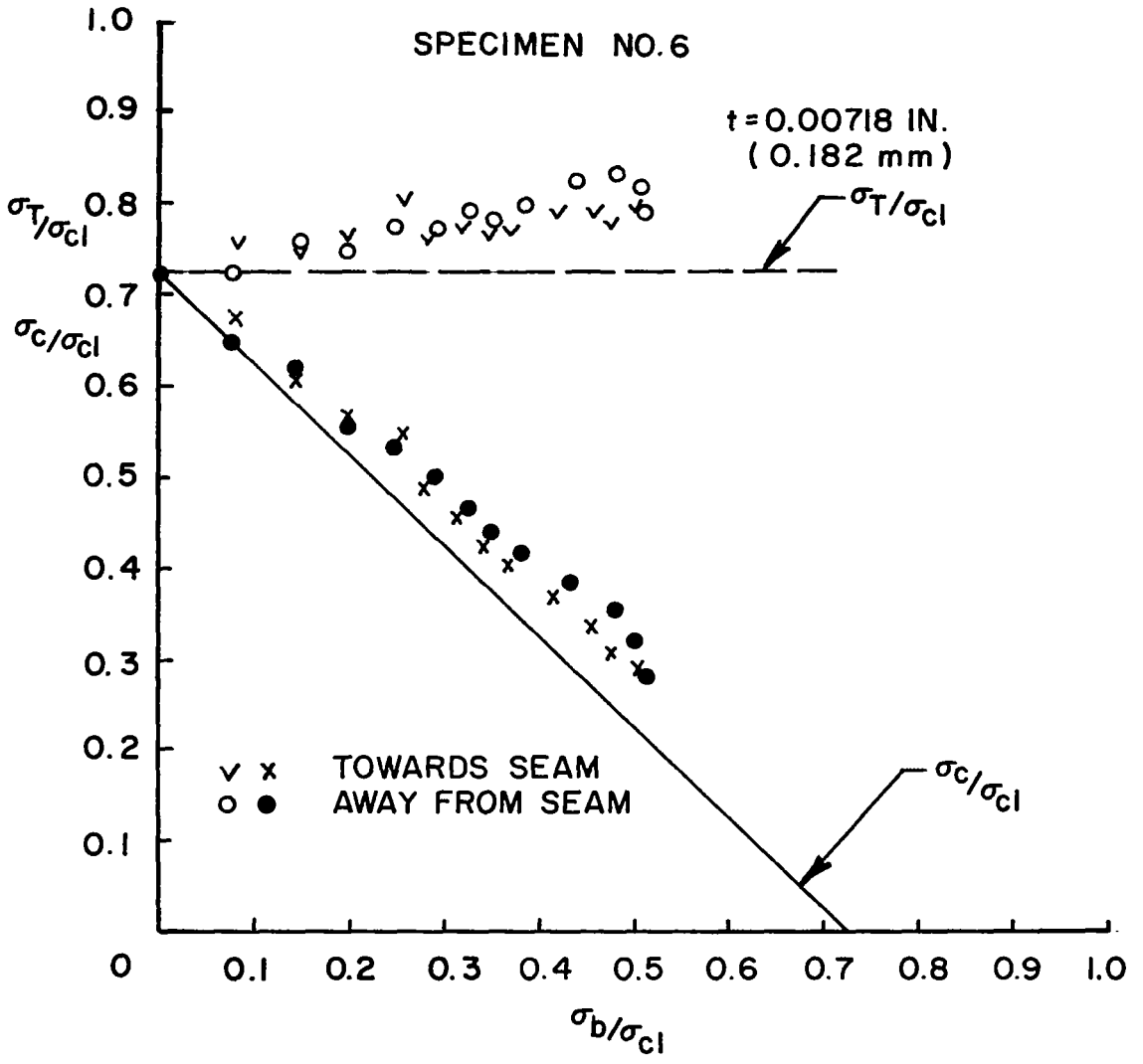

FIG. 20 INTERACTION CURVE

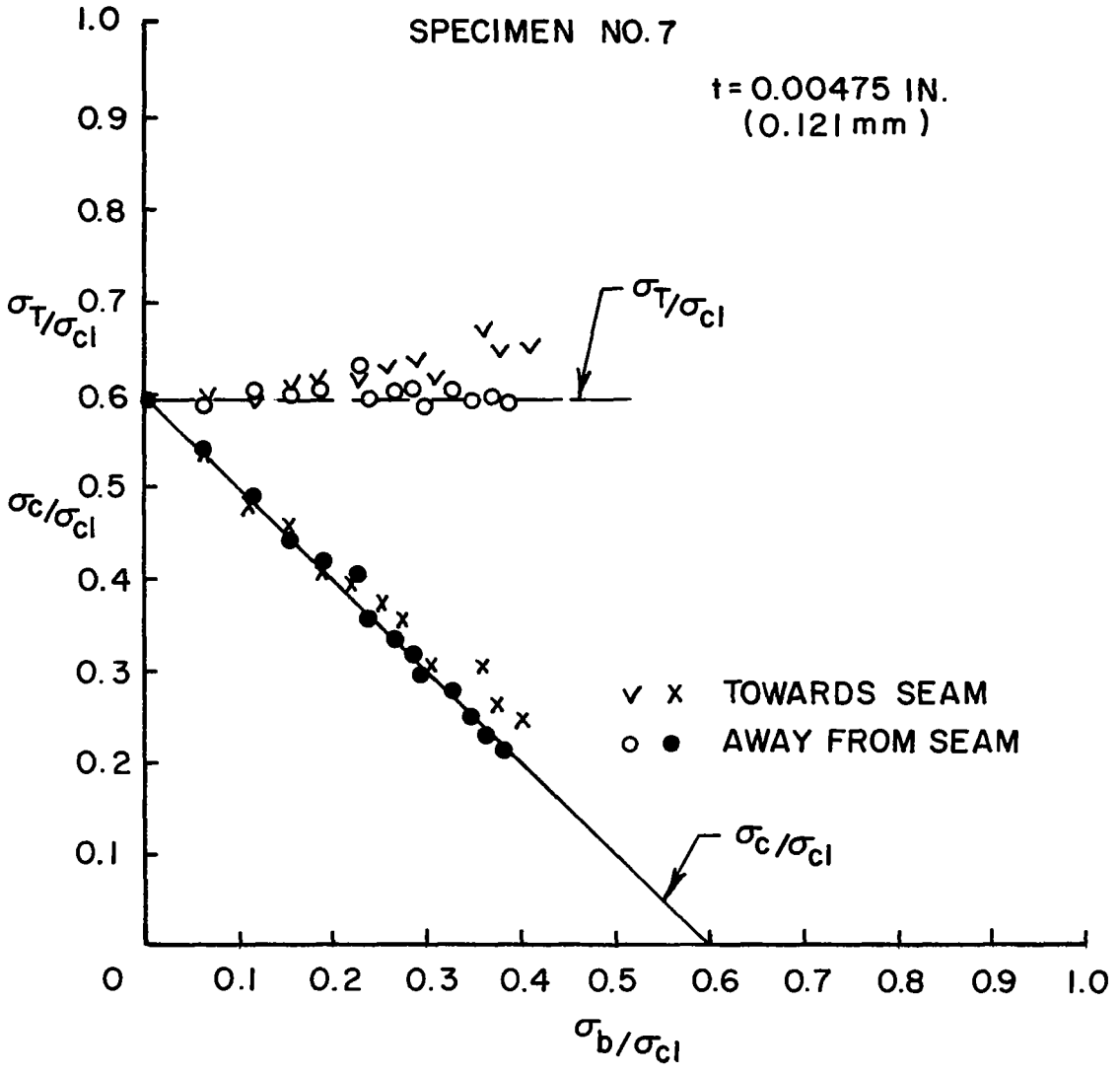

FIG. 21 INTERACTION CURVE

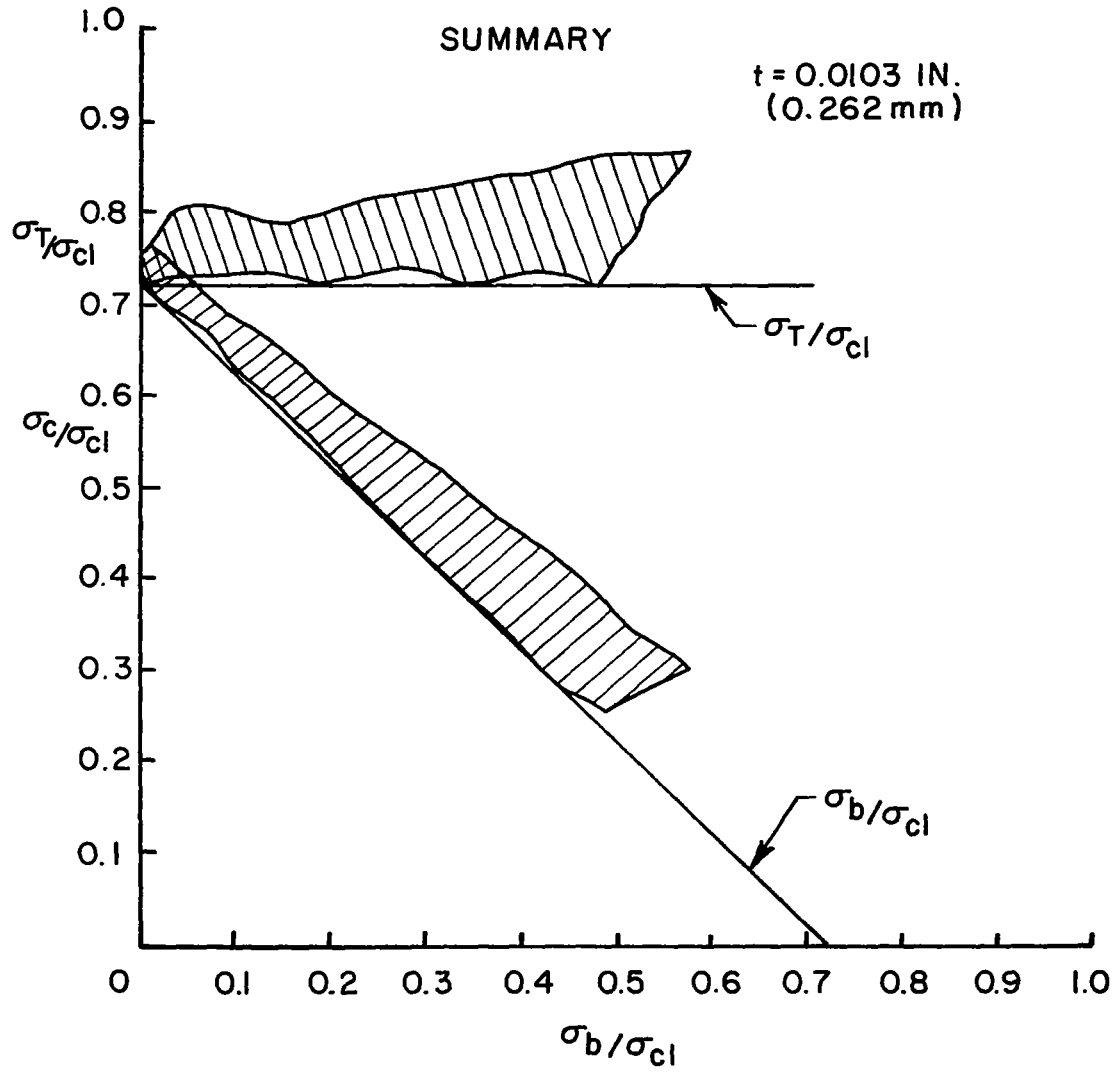

FIG. 22 SUMMARY FOR R/t = 388

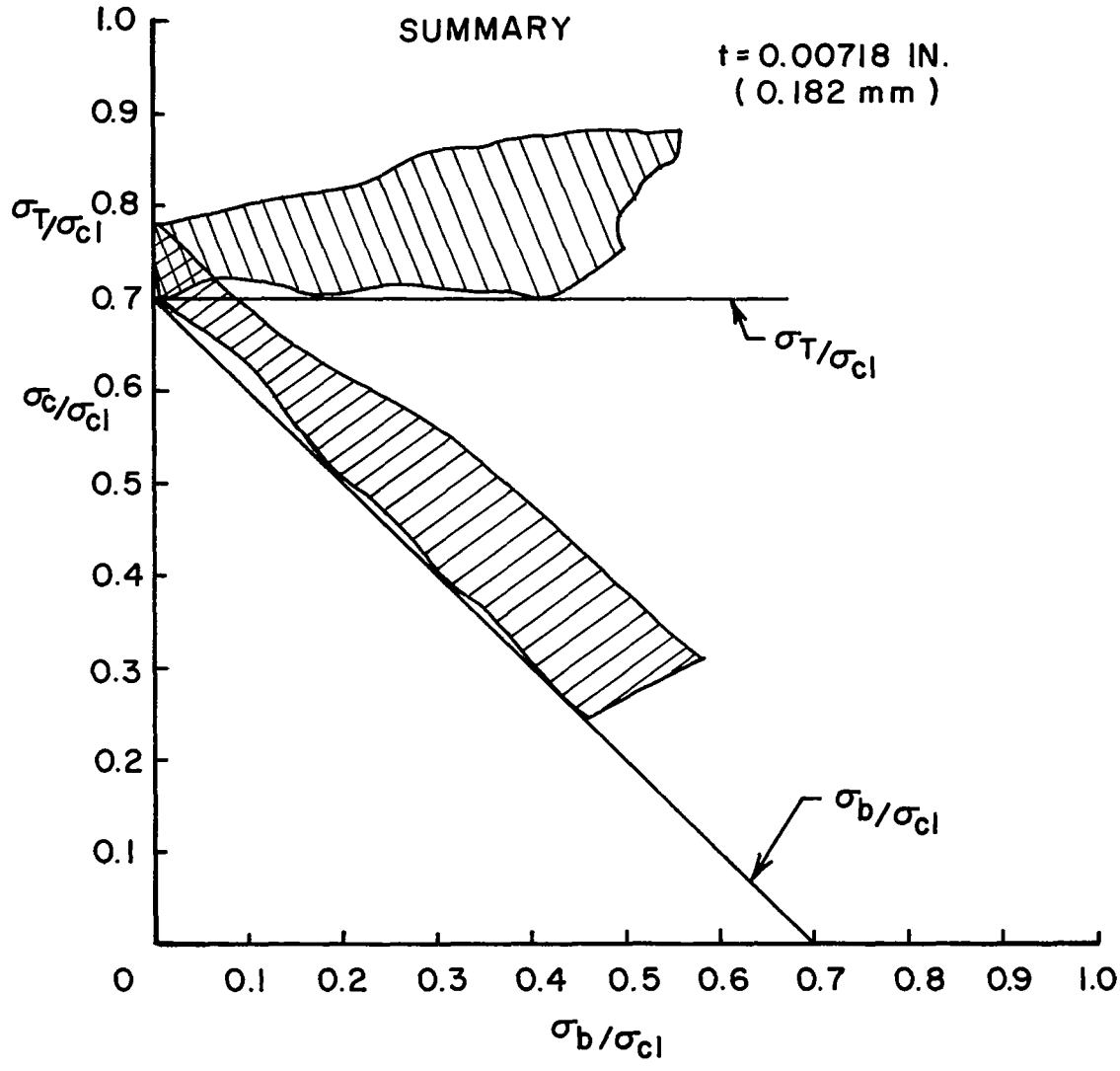

FIG. 23 SUMMARY FOR R/t = 557

Error

An error occurred while processing this page. See the system log for more details.

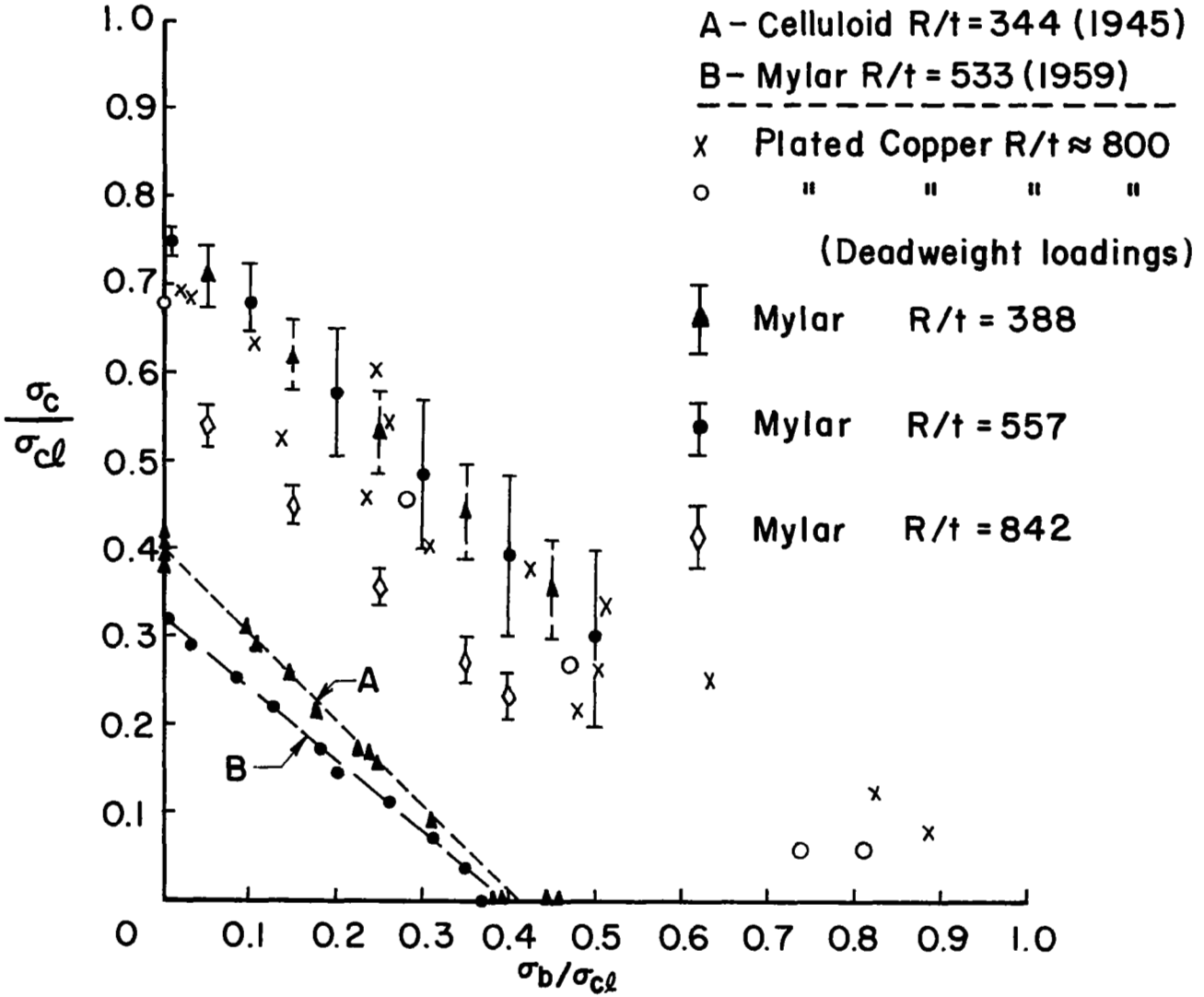

FIG. 25 SUMMARY OF ALL DATA